Succinyl and adipoyl dihydrazones: a solid-state, solution and antibacterial study

Edi Topić,[a] Vladimir Damjanović,[b] Katarina Pičuljan,[a] Višnja Vrdoljak[a], Mirta Rubčić[a]*

[a]University of Zagreb, Faculty of Science, Department of Chemistry, Horvatovac 102a, 10000 Zagreb, Croatia

[b]University of Zagreb, School of Medicine, Department of Chemistry and Biochemistry, Šalata 3, 10000 Zagreb, Croatia

* corresponding author phone: +385(1)4606374; fax +385(1)4606341; e-mail: mirta©chem.pmf.hr

Supplementary Material

Table of Contents

Introduction..... 2
Experimental section..... 2
Single crystal X-ray diffraction..... 2
Results and discussion..... 4
Synthesis and solid-state characterization..... 4
NMR spectroscopy 39

Introduction

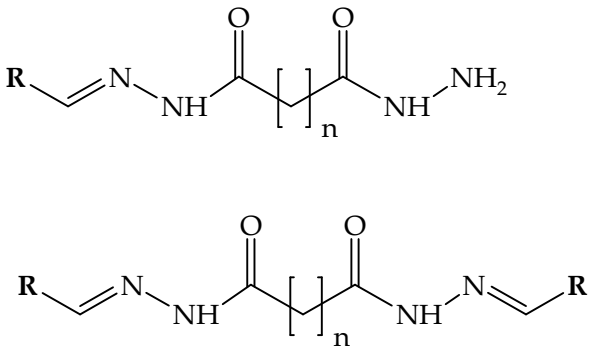

Scheme S1. Mono- and dihydrazone compounds.

Experimental section

Single crystal X-ray diffraction

Table S1. General and crystallographic data for compounds **$H_4L^4 \cdot 2H_2O$**, **H_4L^6** and **H_4L^7**.

Identification code	**$H_4L^4 \cdot 2H_2O$**	**H_4L^6**	**H_4L^7**
Empirical formula	$C_{18}H_{22}N_4O_8$	$C_{28}H_{26}N_4O_4$	$C_{20}H_{22}N_4O_6$
Formula weight	422.39	482.53	414.41
Temperature/K	169.98(10)	169.99(10)	169.99(10)
Crystal system	monoclinic	triclinic	monoclinic
Space group	$P2_1/c$	$P\bar{1}$	$P2_1/c$
a/Å	11.1982(4)	8.6547(6)	11.5192(12)
b/Å	18.0203(6)	9.4387(7)	7.8780(6)
c/Å	9.5584(4)	15.4326(9)	11.7882(11)
α/°	90	84.308(5)	90
β/°	97.763(4)	89.442(5)	117.702(12)
γ/°	90	71.776(7)	90
Volume/Å^3	1911.16(12)	1191.24(15)	947.14(18)
Z	4	2	2
ρ_{calc}/g/cm^3	1.468	1.345	1.453
μ/mm^{-1}	0.996	0.746	0.914
F(000)	888.0	508.0	436.0
Crystal size/mm^3	0.376 × 0.027 × 0.008	0.151 × 0.091 × 0.014	0.045 × 0.023 × 0.014
Radiation	Cu Kα (λ = 1.54184)		
2Θ range for data collection/°	7.968 to 160.366	9.916 to 161.042	8.67 to 158.768
Index ranges	$-14 \le h \le 14$ $-19 \le k \le 22$ $-11 \le l \le 12$	$-11 \le h \le 11$ $-12 \le k \le 12$ $-19 \le l \le 19$	$-14 \le h \le 14$ $-9 \le k \le 9$ $-13 \le l \le 15$
Reflections collected	15137	8953	6778
Independent reflections	3989 [R_{int} = 0.0576, R_{sigma} = 0.0514]	8953 [Merged R_{int}, R_{sigma} = 0.0250]	2013 [R_{int} = 0.0714, R_{sigma} = 0.0659]
Data/restraints/parameters	3989/1/301	8953/0/337	2013/0/145

g_1, g_2 in w	0.0612, 0.5519	0.1867, 0.1663	0.0838, 0.3330
Goodness-of-fit on F^2, S[b]	1.026	1.074	1.096
Final R indexes [I>=2σ (I)][c]	R_1 = 0.0495, wR_2 = 0.1226	R_1 = 0.0845 wR_2 = 0.2330	R_1 = 0.0597, wR_2 = 0.1614
Final R indexes [all data][c]	R_1 = 0.0785, wR_2 = 0.1376	R_1 = 0.1034 wR_2 = 0.2710	R_1 = 0.0896 wR_2 = 0.1839
Largest diff. peak/hole/e Å^{-3}	0.35/–0.24	0.49/–0.39	0.29/–0.31

[a]$w = 1/[\sigma^2(F_o^2) + (g_1P)^2 + g_2P]$ where $P = (F_o^2 + 2F_c^2)/3$

[b]$S = \{\Sigma[w(F_o^2 - F_c^2)^2]/(N_r - N_p)\}^{1/2}$ where N_r = number of independent reflections, N_p = number of refined parameters.

[c]$R = \Sigma||F_o| - |F_c||/ \Sigma|F_o|$; $wR = \{\Sigma[w(F_o^2 - F_c^2)^2]/\Sigma[w(F_o^2)^2]\}^{1/2}$

Results and discussion

Synthesis and solid-state characterization

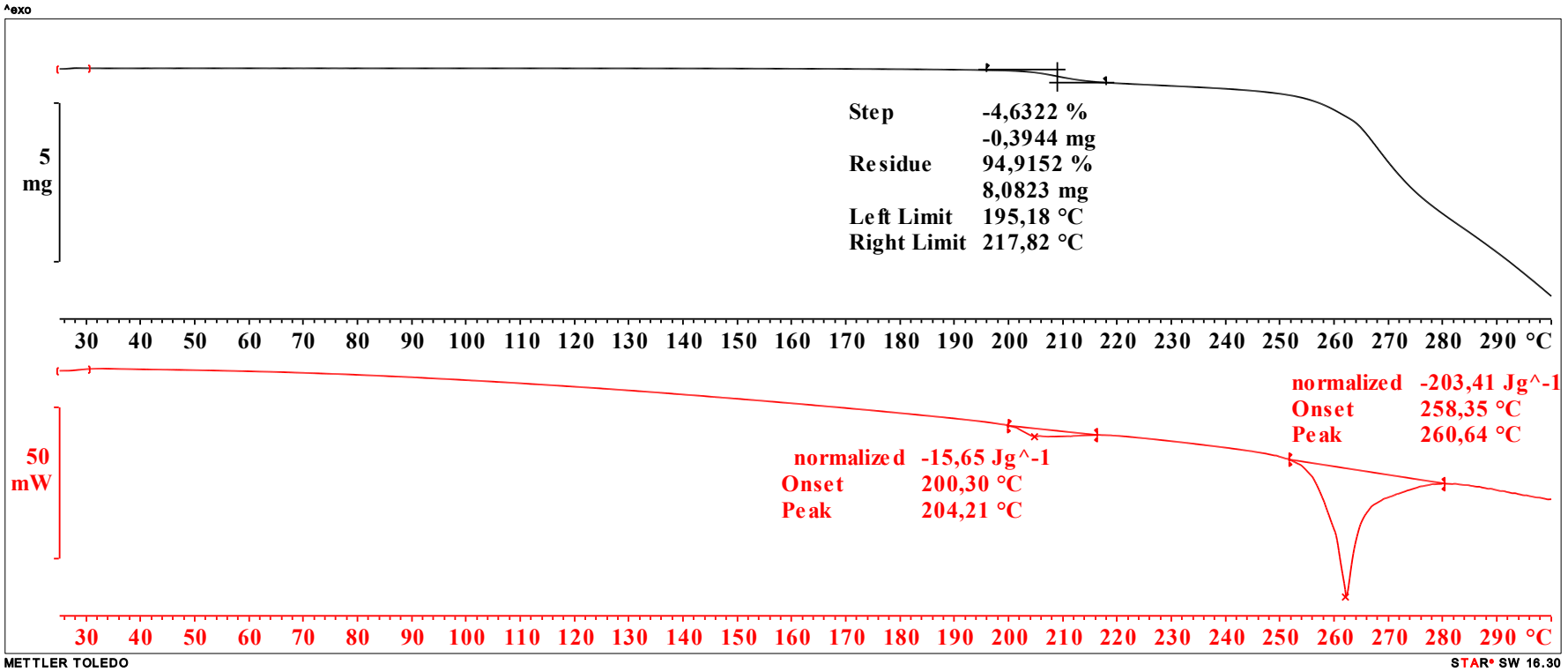

Figure S1. TGA (black) and DSC (red) thermogram of H_4L^1.

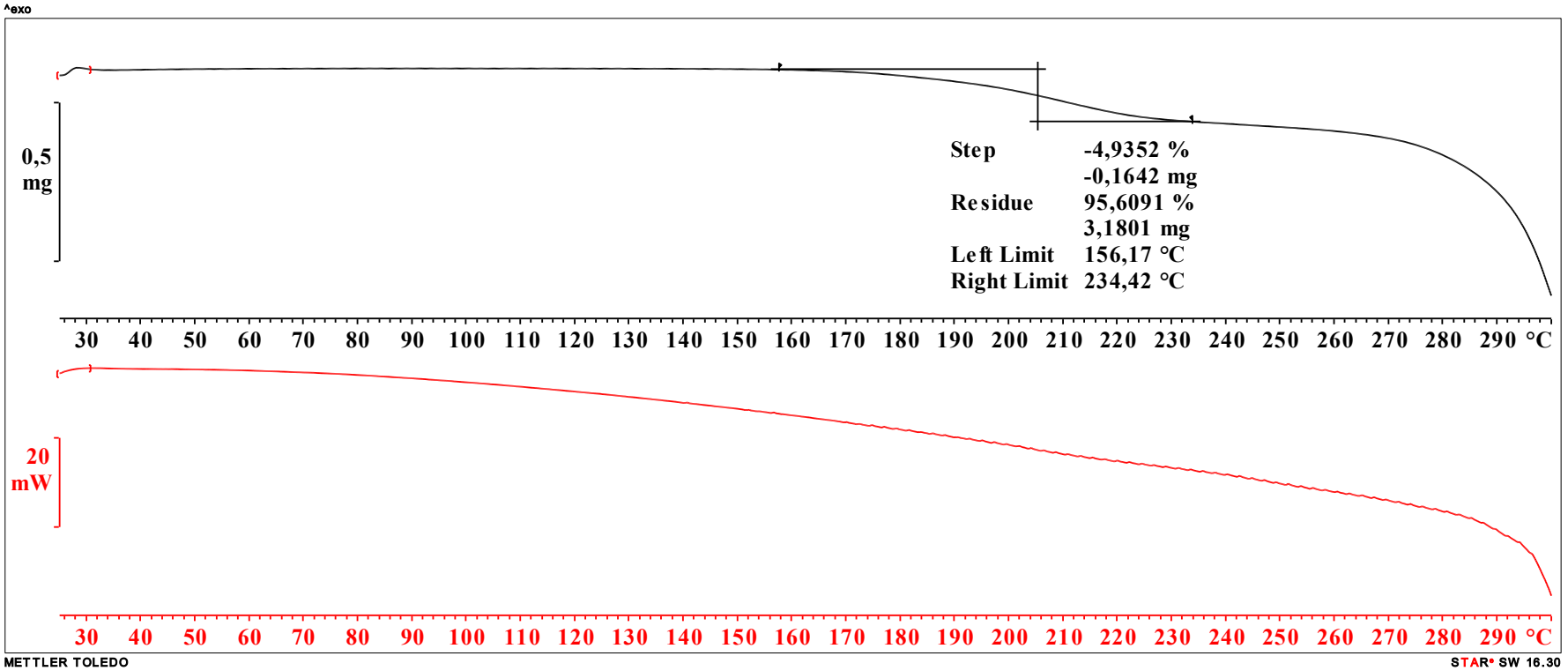

Figure S2. TGA (black) and DSC (red) thermogram of H_4L^2.

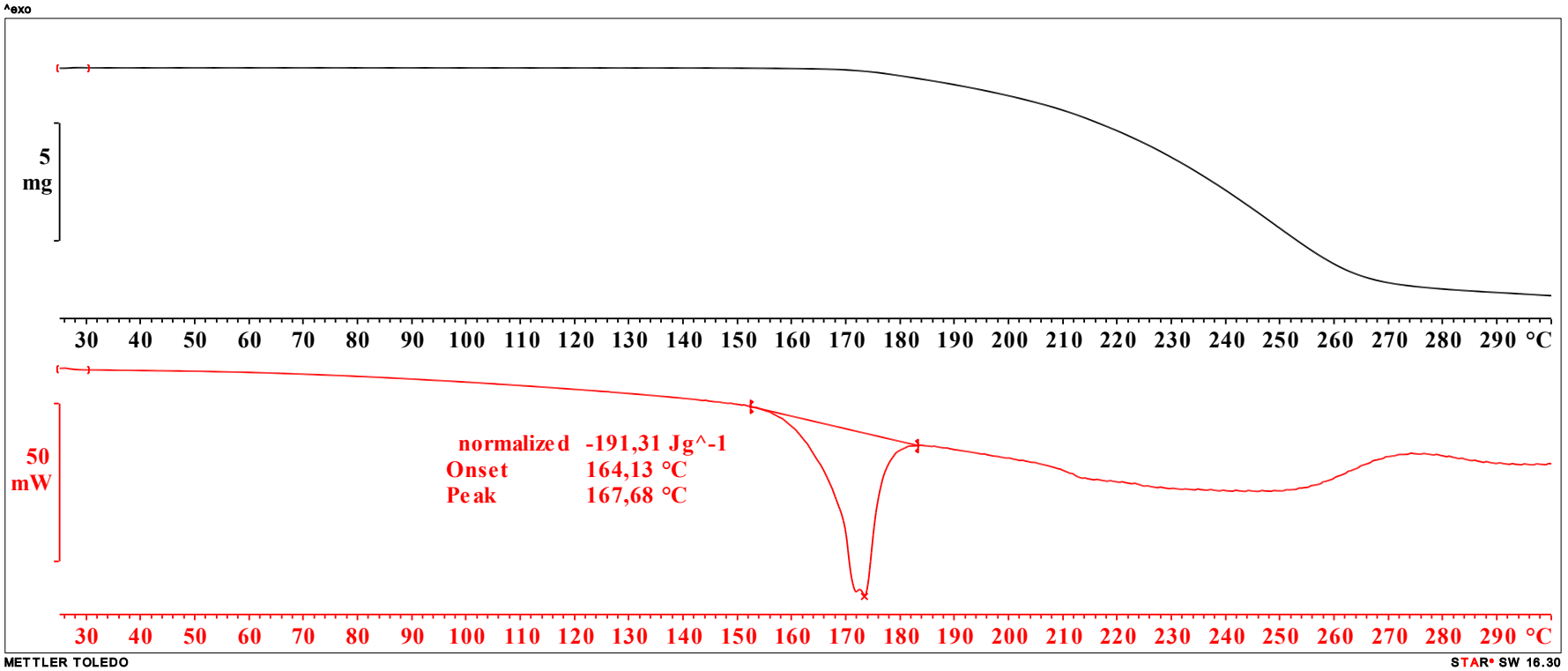

Figure S3. TGA (black) and DSC (red) thermogram of H_4L^3.

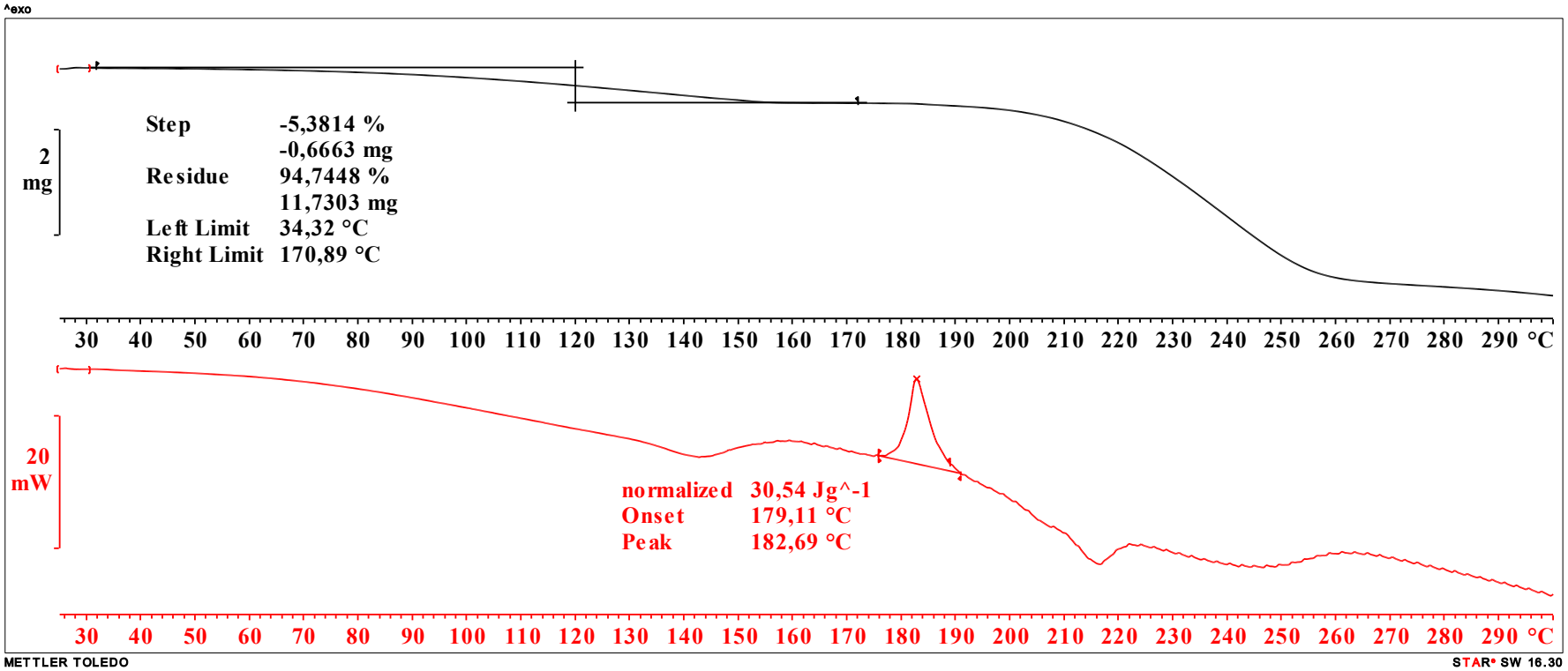

Figure S4. TGA (black) and DSC (red) thermogram of H_4L^4.

Note S1

We believe that the sharp peaks in the DSC curves of investigated compounds could correspond to phase transitions (for the endothermic ones) and crystallization of amorphous phase (for the exothermic ones), but due to events being so close to decomposition temperatures other thermal events (i.e. chemical rearrangements, hydrazone cleavage, polymerization, combinations thereof) cannot be ruled out.

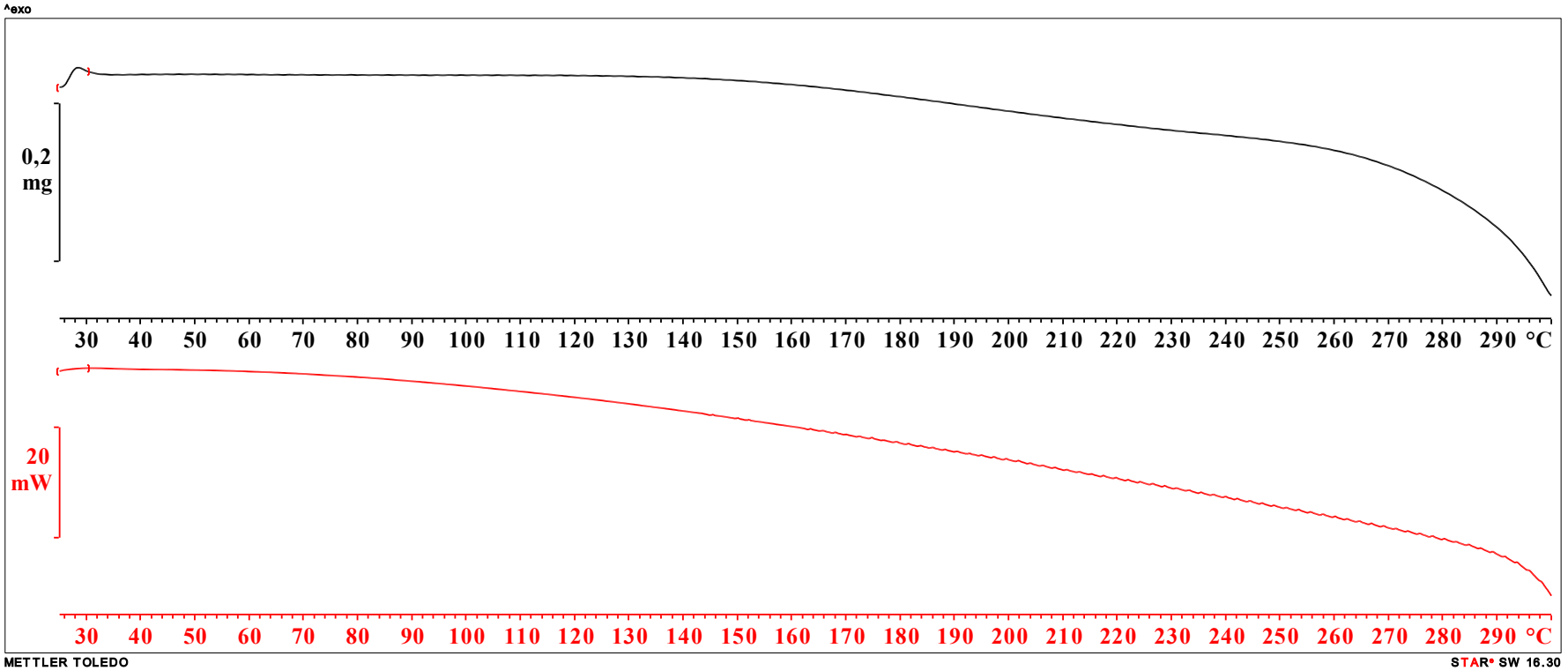

Figure S5. TGA (black) and DSC (red) thermogram of $\mathbf{H_4L^5}$.

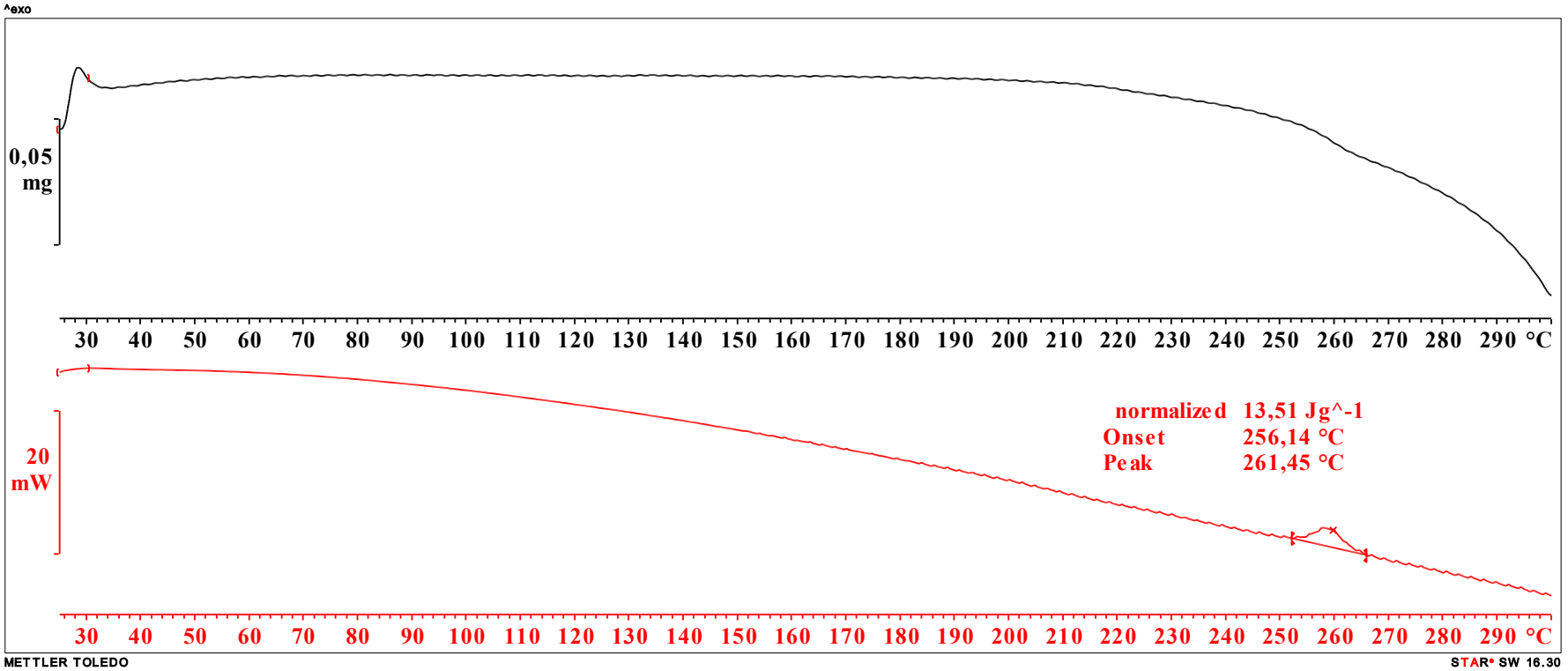

Figure S6. TGA (black) and DSC (red) thermogram of H_4L^6.

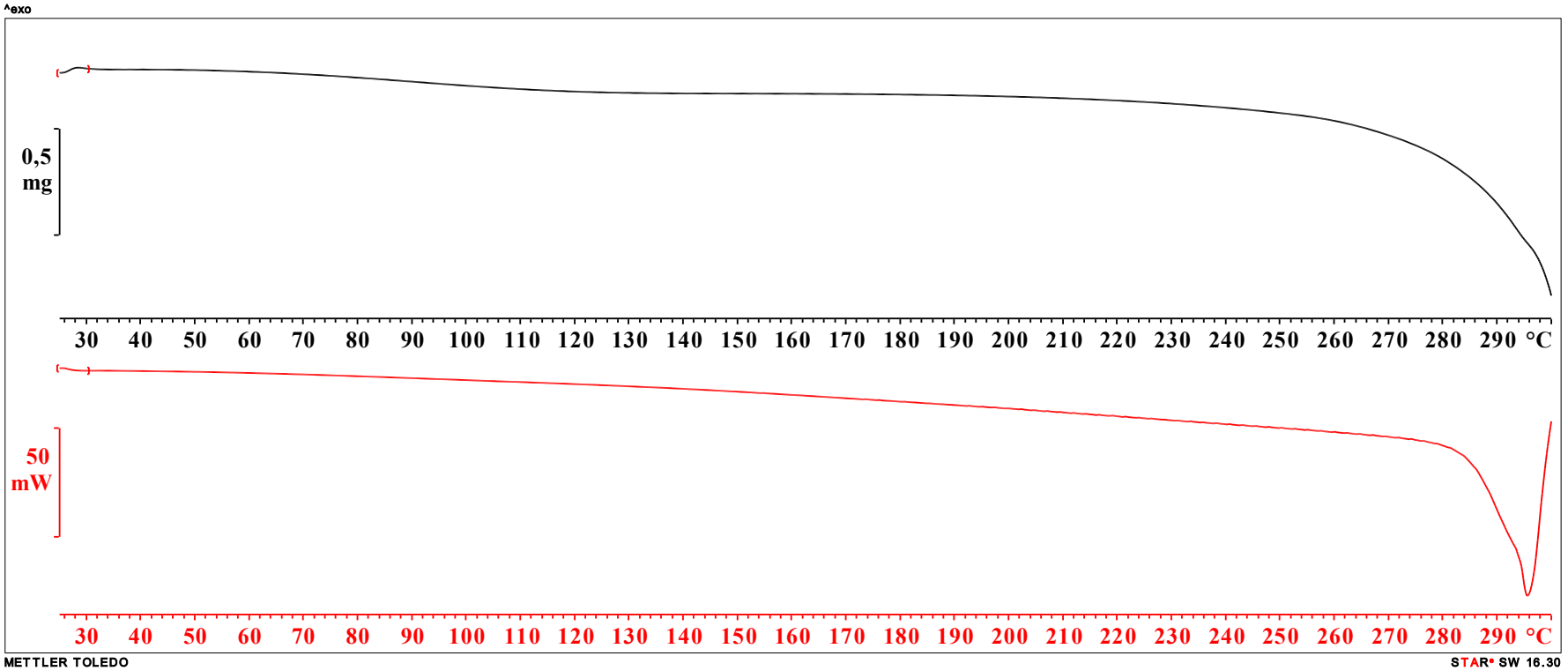

Figure S7. TGA (black) and DSC (red) thermogram of $\mathbf{H_4L^7}$.

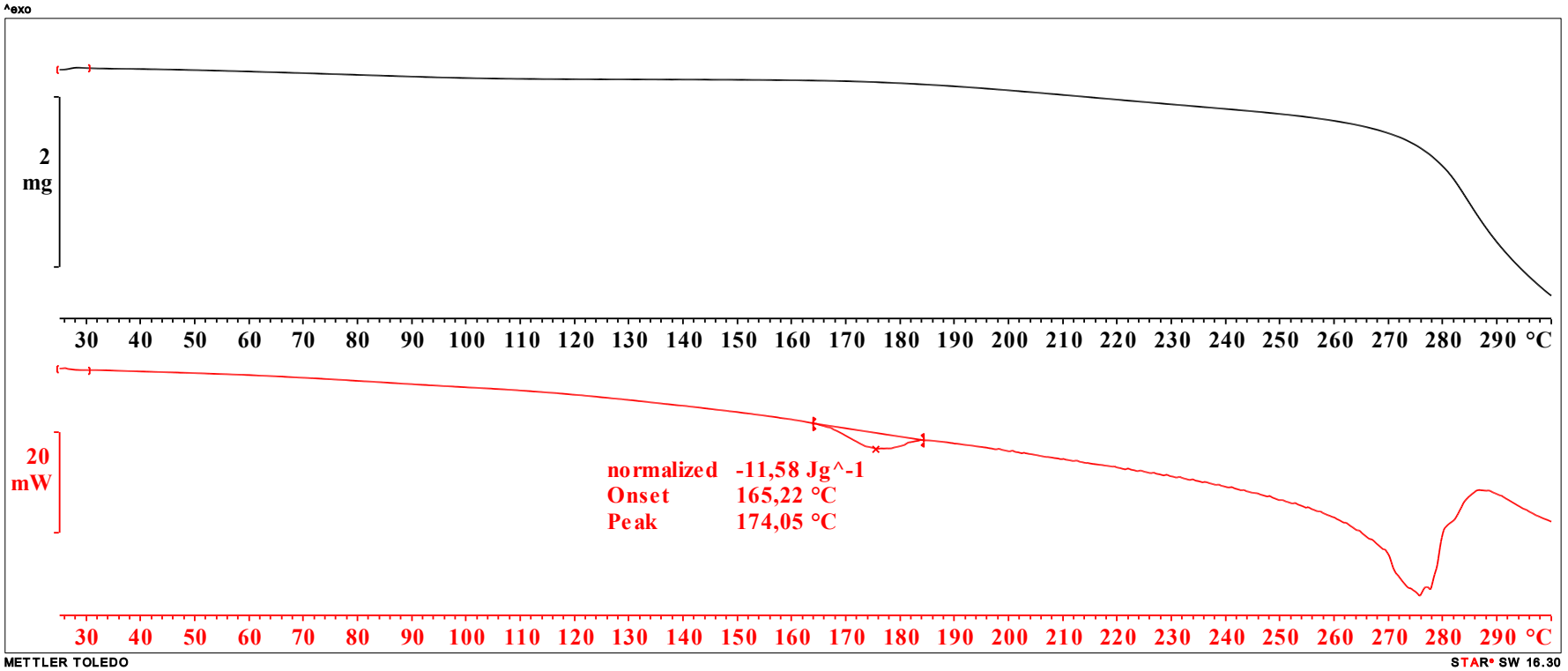

Figure S8. TGA (black) and DSC (red) thermogram of H_4L^8.

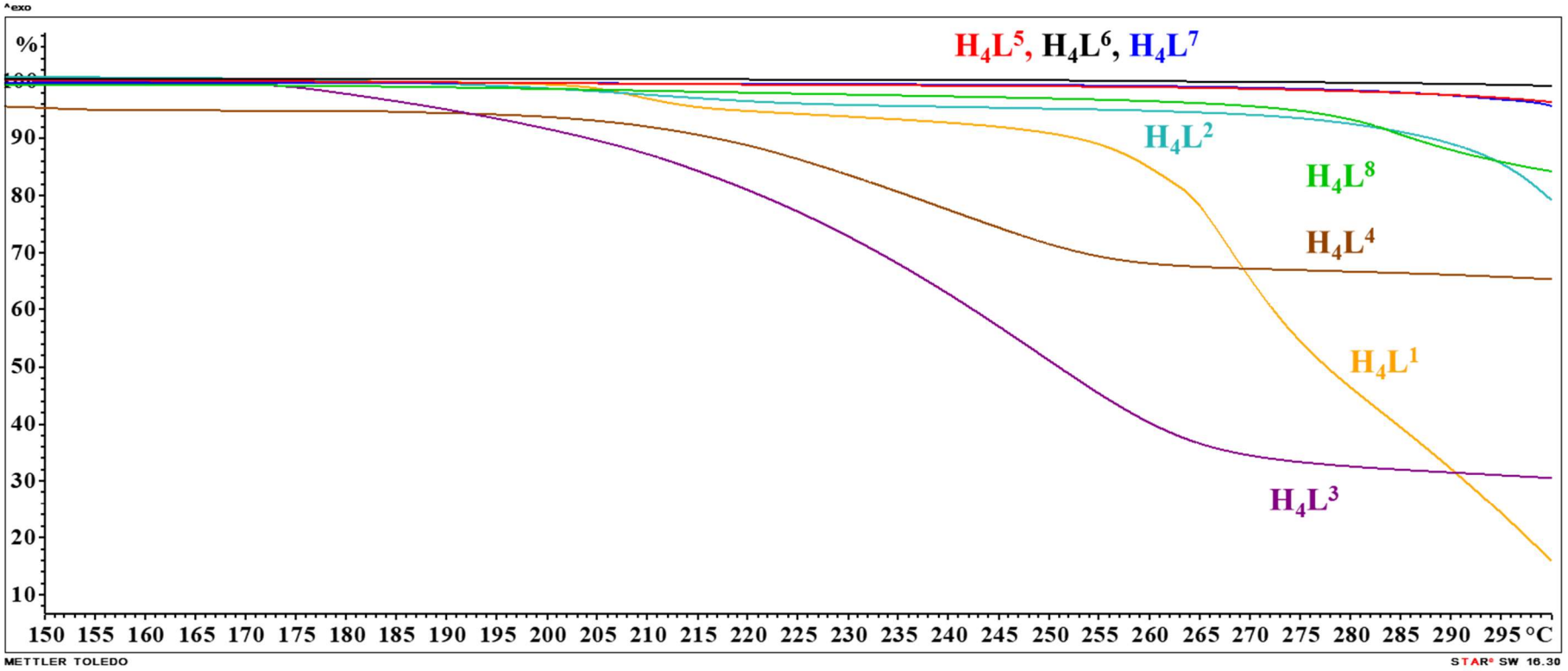

Figure S9. Comparison of TGA thermograms of all eight compounds with common scale.

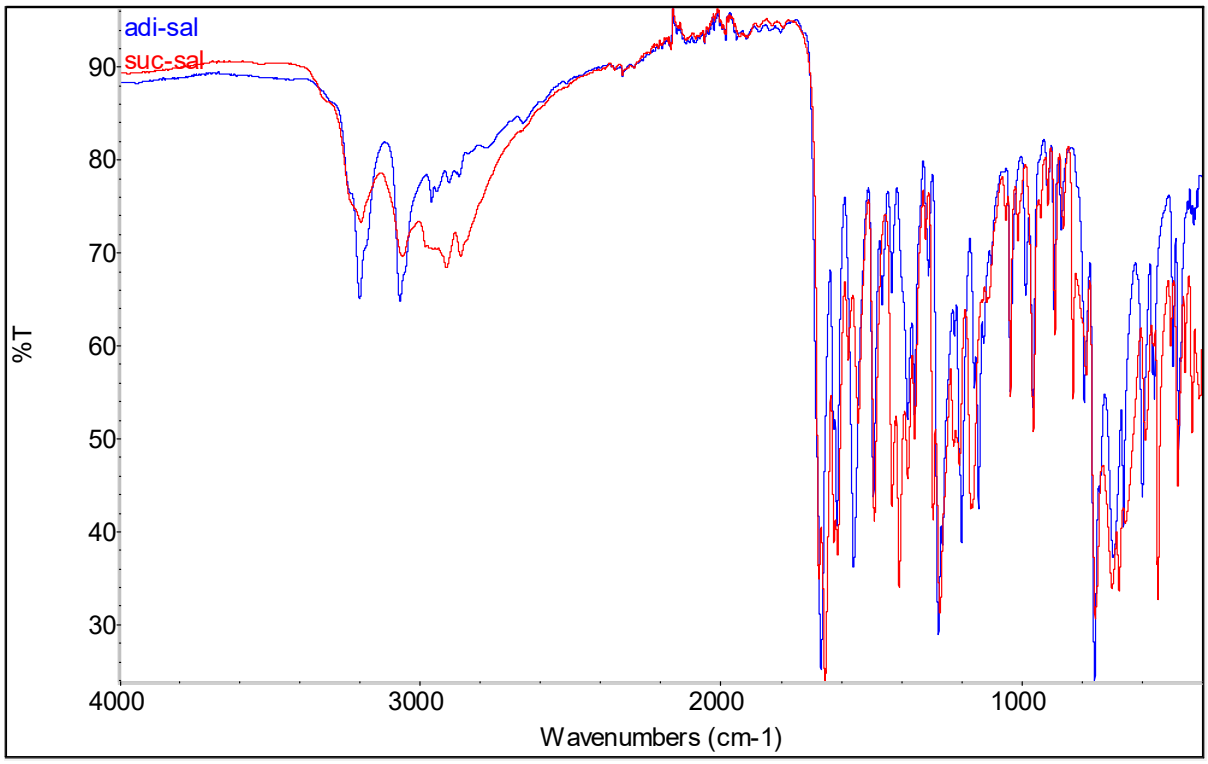

Figure S10. Comparison of ATR-FTIR spectra of $\mathbf{H_4L^1}$ (red) and $\mathbf{H_4L^5}$ (blue) in the full spectral region.

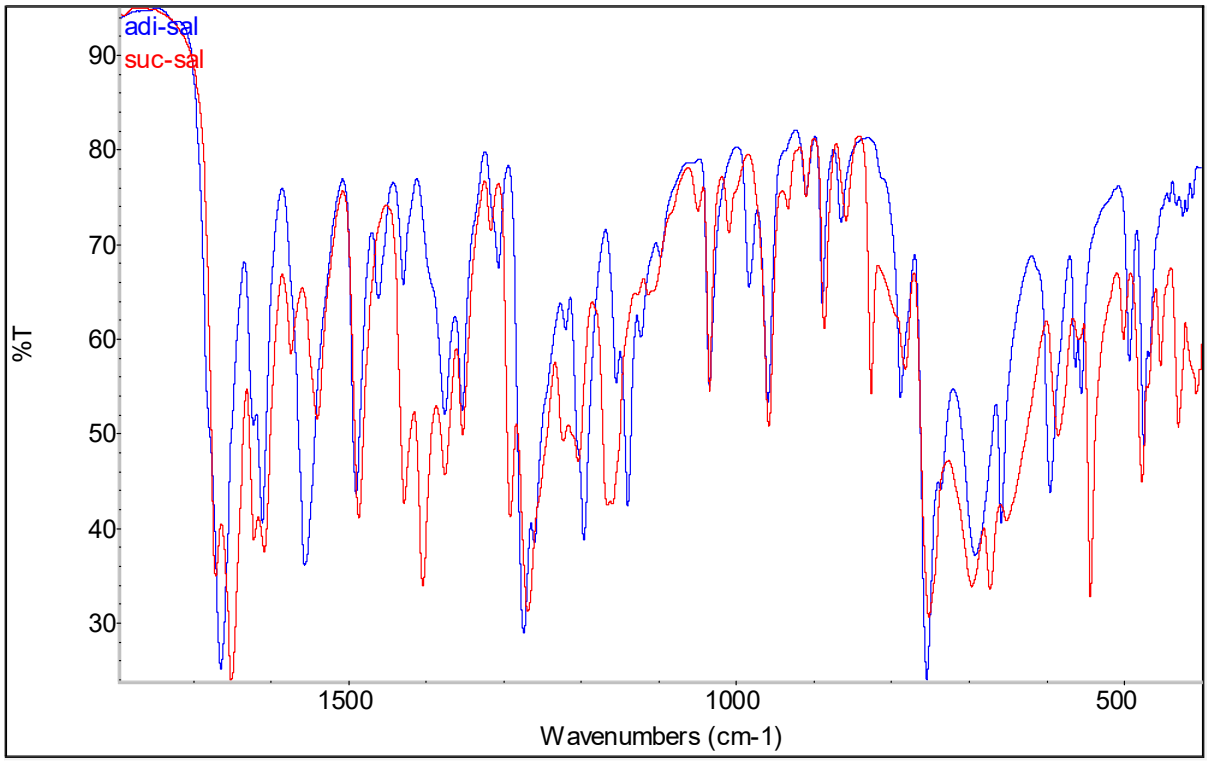

Figure S11. Comparison of ATR-FTIR spectra of $\mathbf{H_4L^1}$ (red) and $\mathbf{H_4L^5}$ (blue) in the region from 1800 to 400 cm^{-1}.

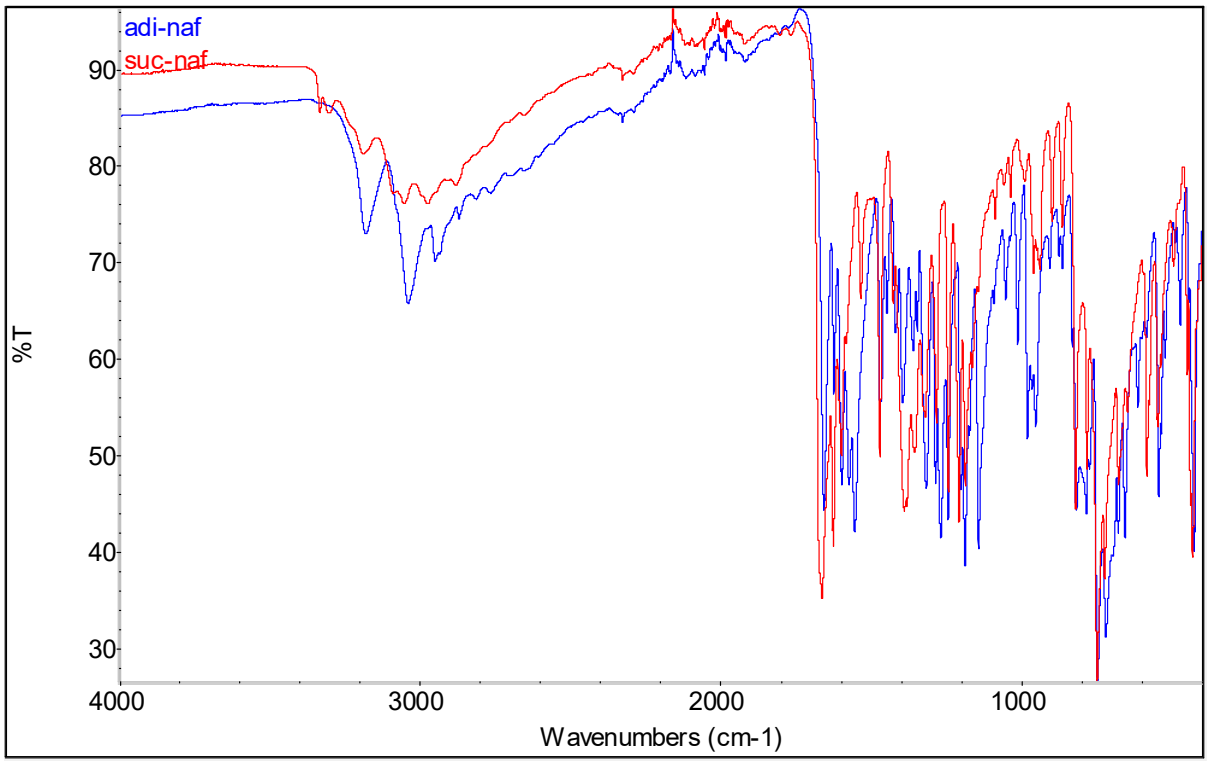

Figure S12. Comparison of ATR-FTIR spectra of $\mathbf{H_4L^2}$ (red) and $\mathbf{H_4L^6}$ (blue) in the full spectral region.

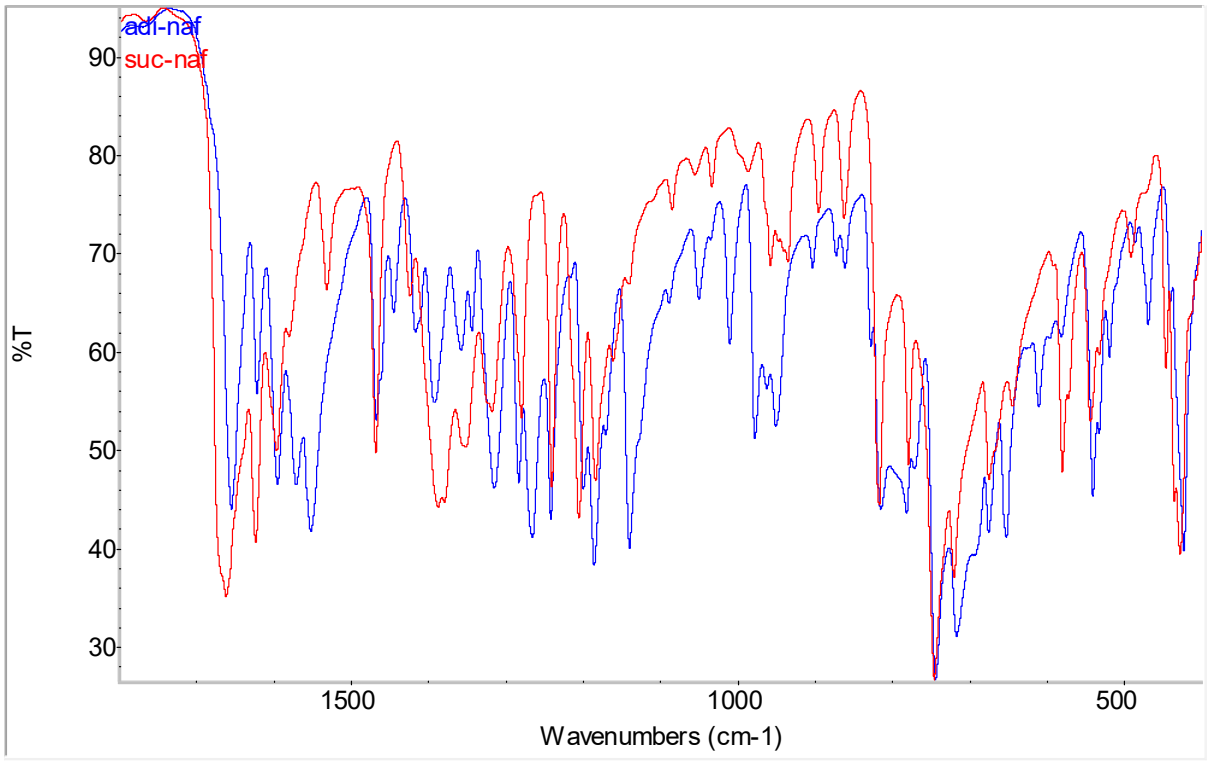

Figure S13. Comparison of ATR-FTIR spectra of $\mathbf{H_4L^2}$ (red) and $\mathbf{H_4L^6}$ (blue) in the region from 1800 to 400 cm^{-1}.

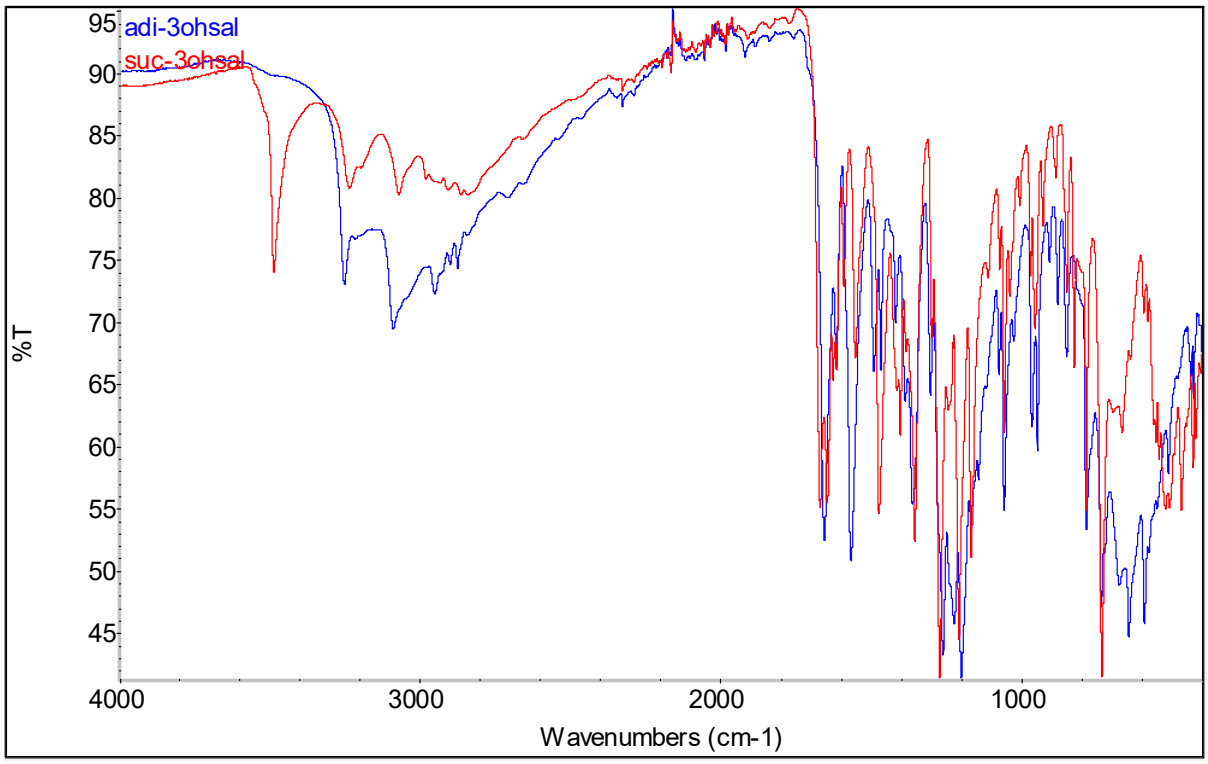

Figure S14. Comparison of ATR-FTIR spectra of $\mathbf{H_4L^3}$ (red) and $\mathbf{H_4L^7}$ (blue) in the full spectral region.

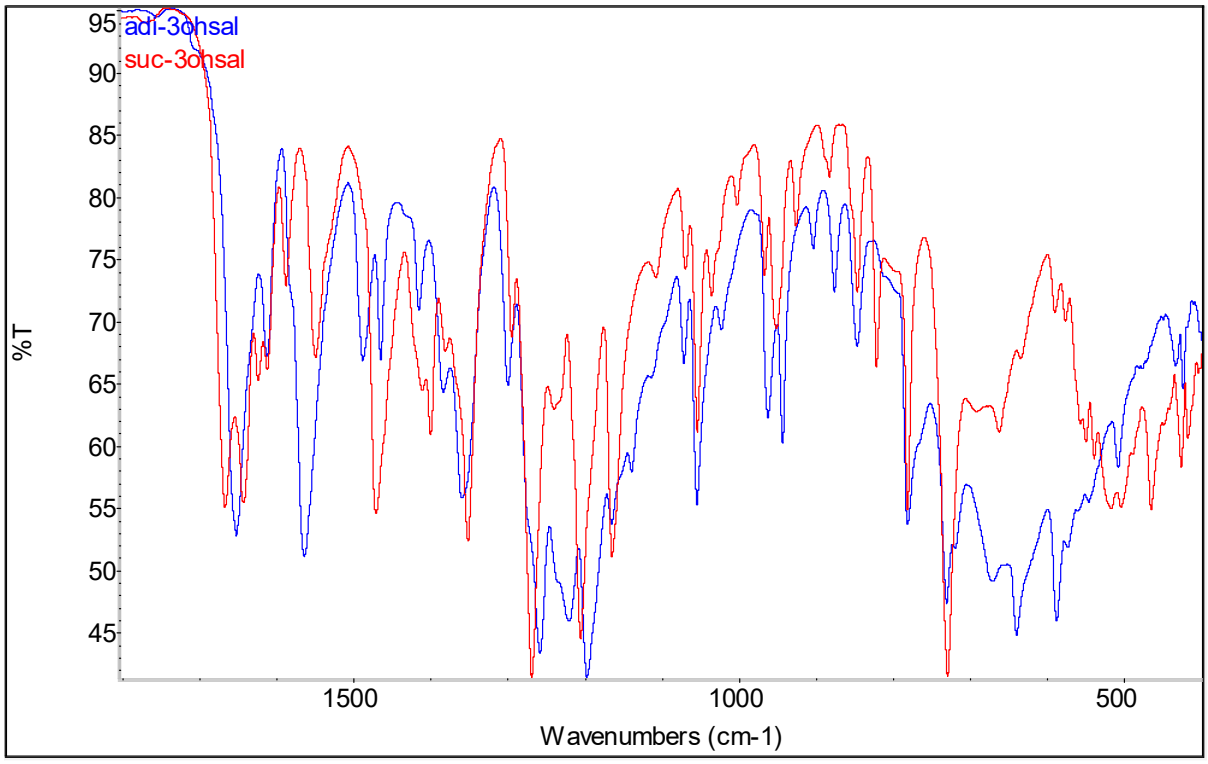

Figure S15. Comparison of ATR-FTIR spectra of $\mathbf{H_4L^3}$ (red) and $\mathbf{H_4L^7}$ (blue)in the region from 1800 to 400 cm^{-1}.

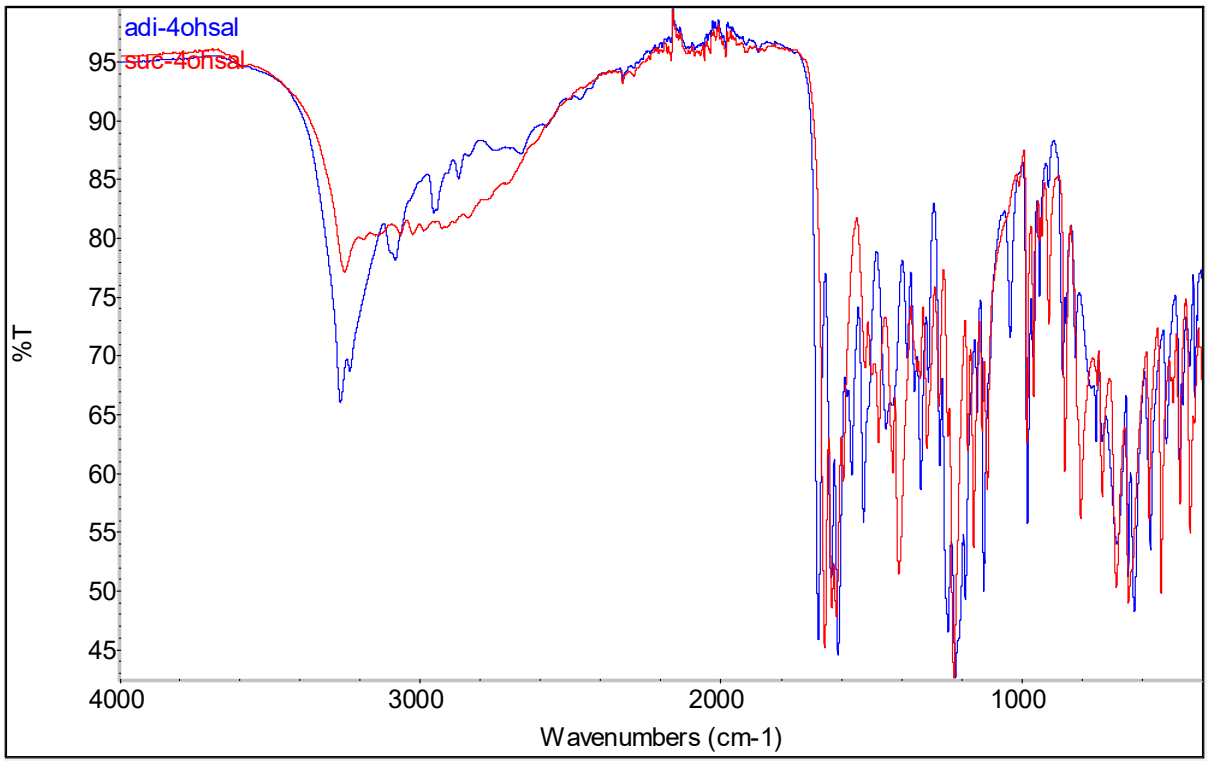

Figure S16. Comparison of ATR-FTIR spectra of $\mathbf{H_4L^4}$ (red) and $\mathbf{H_4L^8}$ (blue) in the full spectral region.

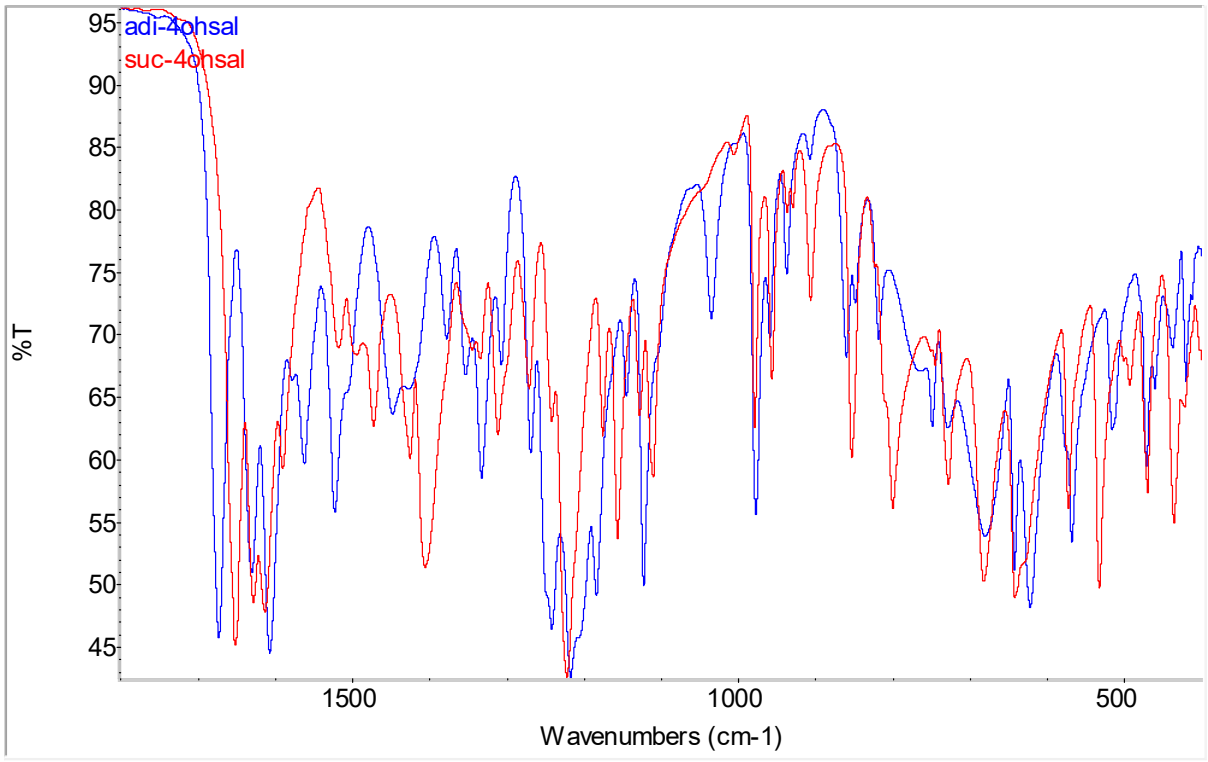

Figure S17. Comparison of ATR-FTIR spectra of $\mathbf{H_4L^4}$ (red) and $\mathbf{H_4L^8}$ (blue) in the region from 1800 to 400 cm^{-1}.

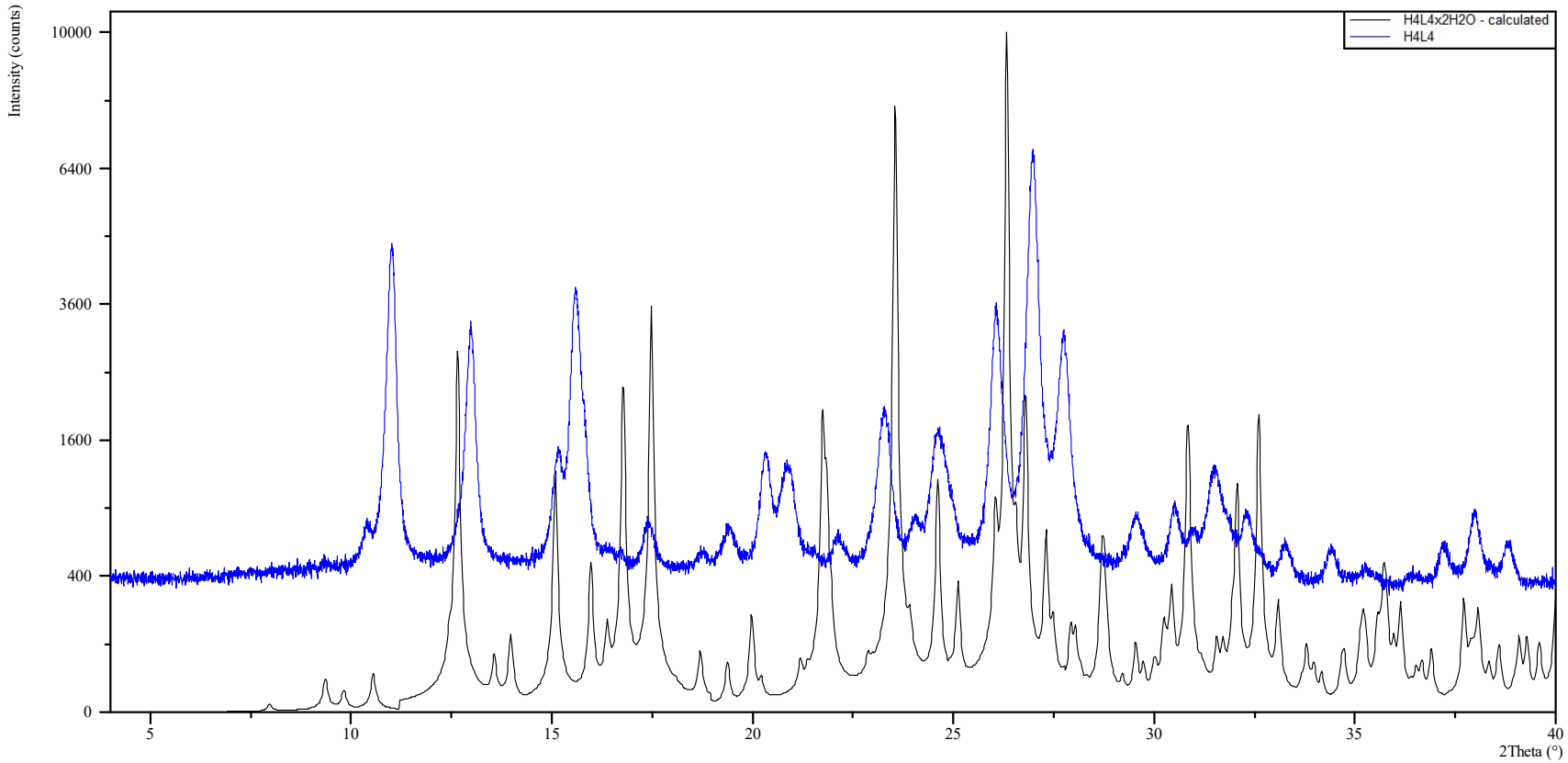

Figure S18. Comparison of PXRD pattern of $\mathbf{H_4L^4}$ and calculated powder pattern from crystal structure of $\mathbf{H_4L^4 \cdot 2H_2O}$. Patterns do not conform well, and it can be concluded that $\mathbf{H_4L^4 \cdot 2H_2O}$ and $\mathbf{H_4L^4}$ indeed have different crystal structures, i.e. they are two different solid phases. Powder pattern of $\mathbf{H_4L^4 \cdot 2H_2O}$ was not measured successfully due to decomposition of the solid form to the anhydrous one.

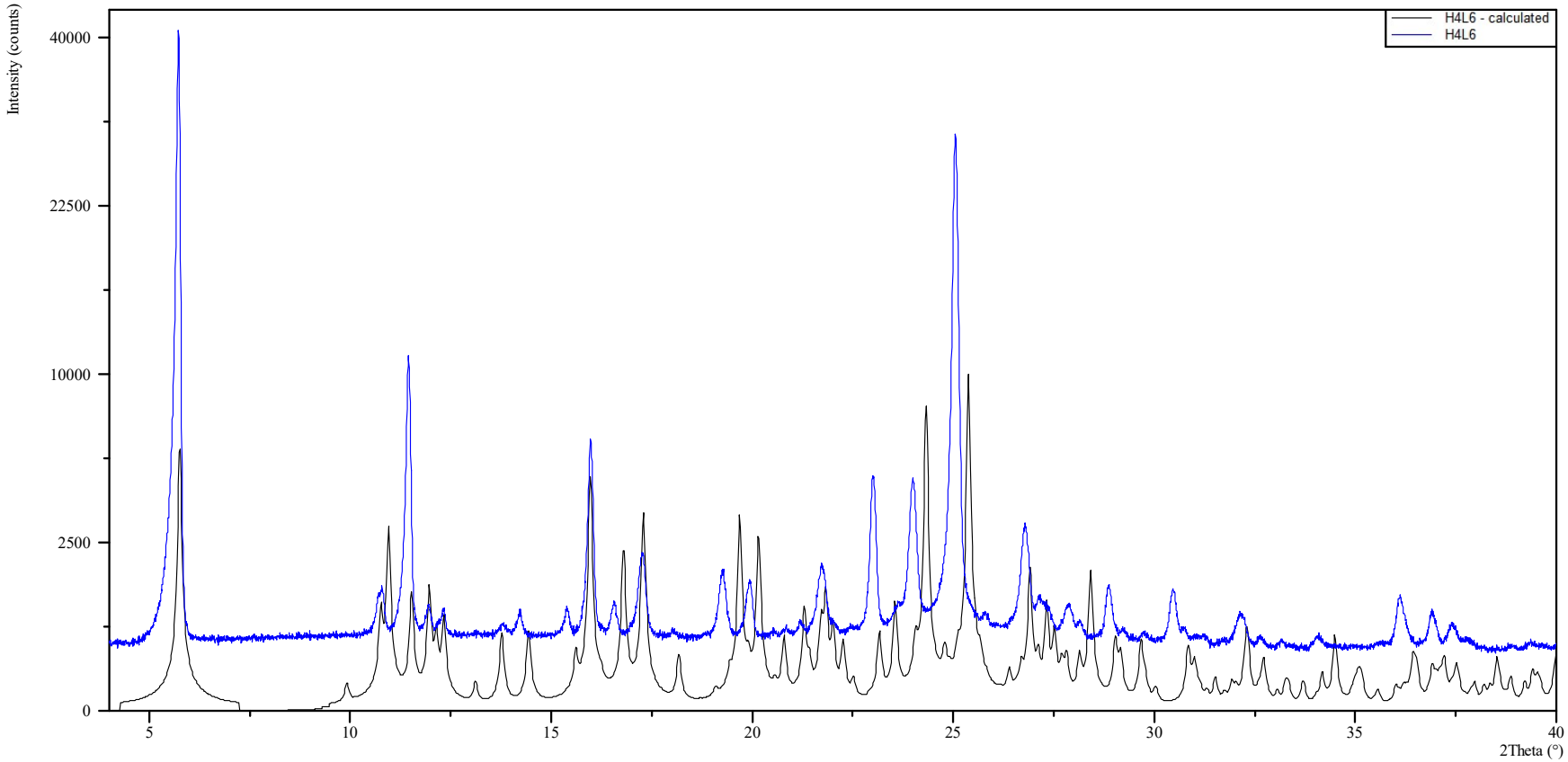

Figure S19. Comparison of PXRD pattern of $\mathbf{H_4L^6}$ and calculated powder pattern from crystal structure of $\mathbf{H_4L^6}$. Patterns conform well to the same compound, albeit powder diffractogram peaks are shifted towards lower angles, which is a consequence of different temperatures for data collection (PXRD: RT, SCXRD: 170 K).

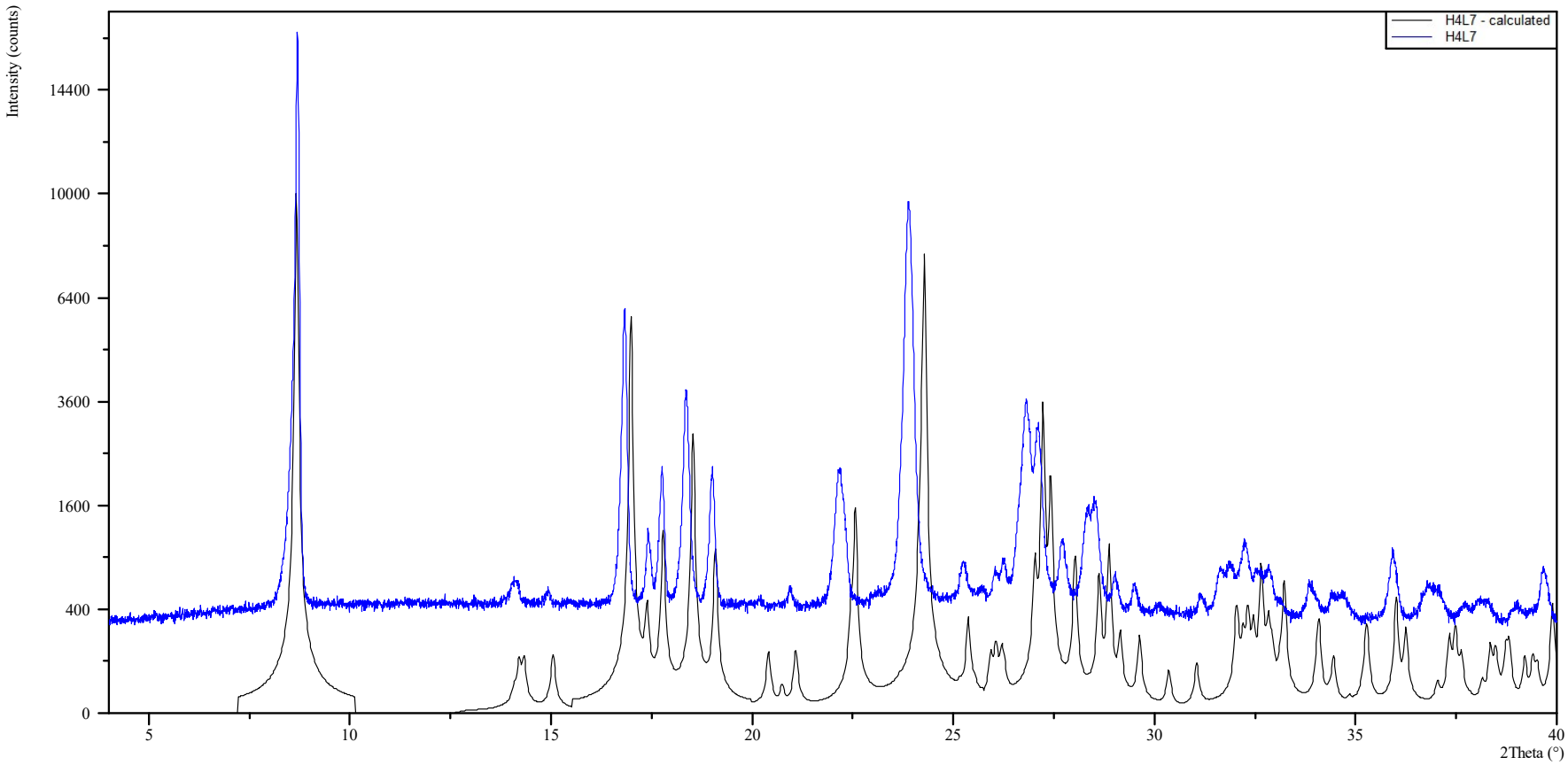

Figure S20. Comparison of PXRD pattern of $\mathbf{H_2L^7}$ and calculated powder pattern from crystal structure of $\mathbf{H_2L^7}$. Patterns conform well to the same compound, albeit powder diffractogram peaks are shifted towards lower angles, which is a consequence of different temperatures for data collection (PXRD: RT, SCXRD: 170 K).

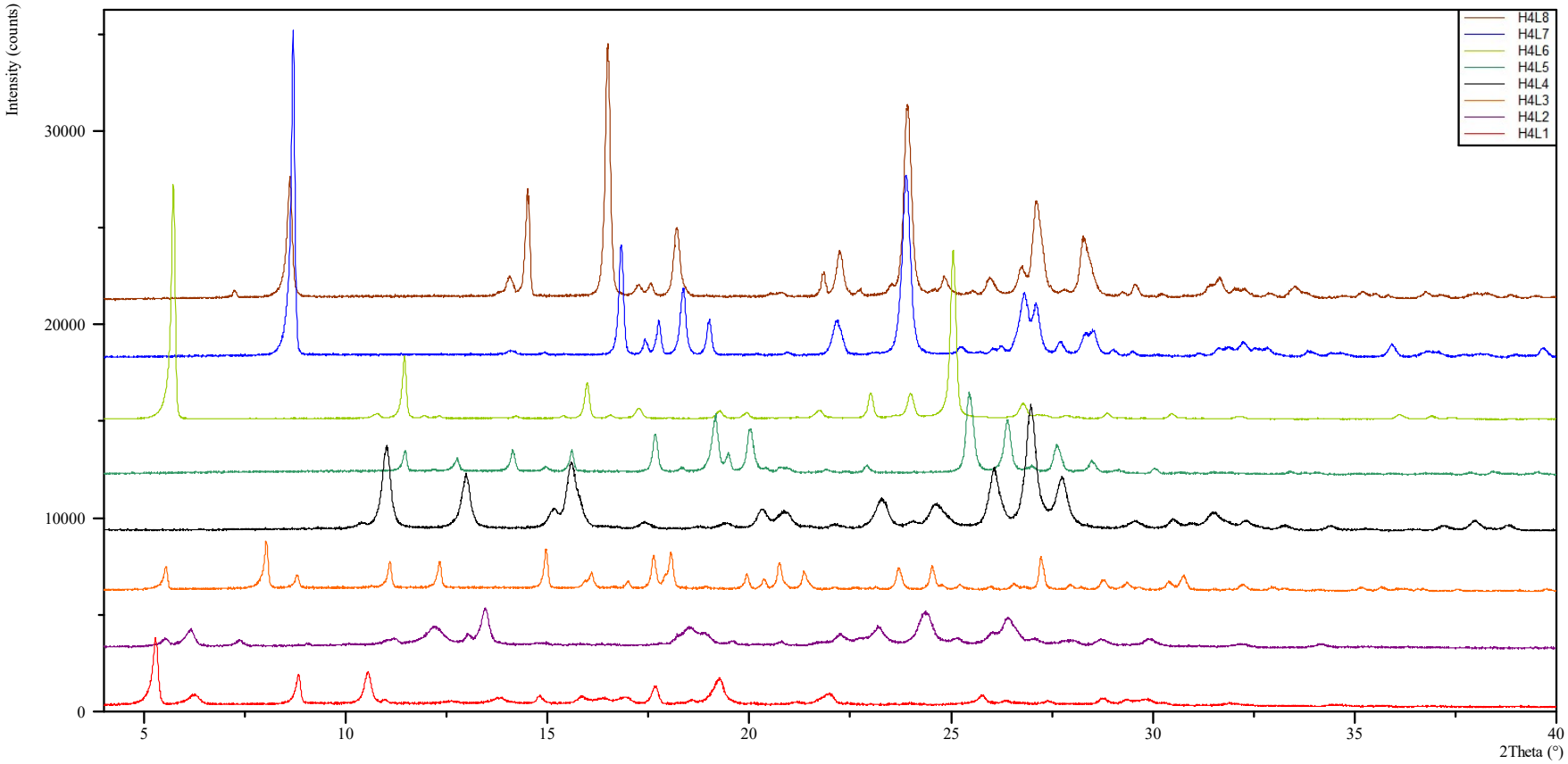

Figure S21. Comparison of PXRD patterns for obtained dihydrazones.

Note S2

Measurement of the crystal structure of **H_4L^2** yielded essentially identical structure to the one reported in the literature (see reference 39, main text). Comparison of cell parameters is given below.

	a/Å	*b*/Å	*c*/Å	*α*/°	*β*/°	*γ*/°	*V*/ Å^3	SG
Measured (170 K)	20.1473(13)	4.5802(6)	17.4119(12)	90	114.620(10)	90	1460.7	$P2_1/c$
Reported (RT)	20.119(2)	4.631(1)	17.522(1)	90	114.68(1)	90	1483.4	$P2_1/c$

It can be concluded that the structures are essentially identical, with small differences due to different measurement temperatures.

Table S2. Bond lengths (in Å) for **$H_4L^4 \cdot 2H_2O$, H_4L^6** and **H_4L^7**. Atoms are numerated according to Figures S22-S24.

Bond	**$H_4L^4 \cdot 2H_2O$**		**H_2L^6**		**H_4L^7**
	part 1	*part 2*	*residue 1*	*residue 2*	
C1–C2	1.402(3)	1.410(3)	1.390(4)	1.398(5)	1.398(3)
C1–C6	1.401(3)	1.407(3)	1.442(4)	1.443(5)	1.398(5)
C1–C7	1.447(3)	1.440(3)	1.452(4)	1.453(4)	1.452(4)
C2–C3	1.390(3)	1.391(3)	1.411(5)	1.407(5)	1.399(4)
C3–C4	1.401(3)	1.396(3)	1.358(5)	1.355(6)	1.369(5)
C4–C5	1.384(3)	1.389(3)	1.425(5)	1.421(6)	1.402(4)
C5–C11			1.413(5)	1.403(6)	
C5–C6	1.370(3)	1.373(3)	1.425(4)	1.422(5)	1.369(5)
C6–C14			1.418(4)	1.414(5)	
C8–C9	1.505(3)	1.509(3)	1.514(4)	1.499(4)	1.511(4)
C9–C10			1.520(4)	1.541(5)	1.520(3)
C10–C10(a)	1.513(3)		1.524(4)	1.525(4)	1.533(4)
C11–C12			1.357(6)	1.365(7)	
C12–C13			1.403(5)	1.407(6)	
C13–C14			1.373(5)	1.371(5)	
N1–N2	1.384(3)	1.392(3)	1.370(4)	1.379(4)	1.373(3)
N1–C7	1.285(3)	1.284(3)	1.288(4)	1.284(4)	1.279(3)
N2–C8	1.324(3)	1.321(3)	1.349(4)	1.357(4)	1.343(3)
O1–C2	1.365(3)	1.362(3)	1.354(4)	1.350(4)	1.359(3)
O2–C8	1.242(2)	1.244(3)	1.223(3)	1.225(3)	1.235(3)
O3–C3					1.361(3)
O3–C4	1.354(3)	1.355(3)			

Table S3. Bond angles (in Å) for **$H_4L^4 \cdot 2H_2O$, H_4L^6** and **H_4L^7**. Atoms are numerated according to Figures S22-S24.

Angle	**$H_4L^4 \cdot 2H_2O$**		**H_4L^6**		**H_4L^7**
	part 1	*part 2*	*residue 1*	*residue 2*	
C2–C1–C7	122.97(19)	123.93(19)	120.6(3)	120.2(3)	121.7(3)
C6–C1–C7	119.6(2)	118.6(2)	119.9(2)	119.7(3)	119.6(2)
C2–C1–C6	117.39(19)	117.5(2)	119.5(3)	120.1(3)	118.7(3)
O1–C2–C3	117.73(19)	117.79(19)	116.2(3)	116.4(3)	117.3(2)
C1–C2–C3	120.84(19)	120.79(19)	120.8(3)	120.3(3)	120.1(2)
O1–C2–C1	121.43(18)	121.41(19)	123.0(3)	123.3(3)	122.6(3)
C2–C3–C4	119.5(2)	119.6(2)	120.1(3)	120.3(4)	119.9(2)
O3–C3–C4	122.05(19)*	122.2(2)*			124.0(3)
O3–C3–C2	117.5(2)*	117.3(2)*			116.2(3)
C3–C4–C5	120.4(2)	120.6(2)	122.1(3)	122.1(3)	120.7(3)
C6–C5–C11			119.7(3)	119.4(4)	
C4–C5–C6	119.1(2)	119.3(2)	118.4(3)	118.5(4)	119.3(3)
C4–C5–C11			121.9(3)	122.1(3)	
C5–C6–C14			116.9(3)	117.2(3)	
C1–C6–C5	122.6(2)	122.3(2)	119.1(3)	118.8(3)	121.3(3)
C1–C6–C14			123.9(3)	124.0(3)	
N1–C7–C1	121.8(2)	122.4(2)	120.7(3)	120.6(3)	121.7(2)
O2–C8–C9	120.89(19)	121.0(2)	124.5(3)	123.4(3)	122.6(2)
N2–C8–C9	115.40(18)	115.63(19)	112.6(2)	115.1(3)	113.85(19)
O2–C8–N2	123.70(19)	123.4(2)	123.0(3)	121.5(3)	123.5(2)
C8–C9–C10			113.9(2)	112.4(3)	113.52(19)
C9–C10–C10(a)	111.69(18)*	111.32(19)*	111.1(2)	113.9(3)	111.79(19)
C5–C11–C12			121.6(3)	122.0(4)	
C11–C12–C13			119.4(4)	119.2(4)	
C12–C13–C14			120.6(3)	119.9(4)	
C6–C14–C13			121.7(3)	122.2(3)	
N2–N1–C7	115.23(18)	114.21(18)	116.6(3)	117.5(3)	116.4(2)
N1–N2–C8	120.80(17)	121.14(18)	120.7(3)	118.4(3)	120.7(2)

Table S4. Geometric parameters of hydrogen bonds present in the structures of $H_4L^4 \cdot 2H_2O$ H_4L^6 and H_4L^7. Atoms are numerated according to Figures S22-S24.

D–H···A	D–H	H···A	D···A	∠D–H···A	Symmetry code
$H_4L^4 \cdot 2H_2O$					
O1–H1···N1	0.91(3)	1.83(3)	2.649(2)	149(3)	
O1A–H1A···N1A	0.88(3)	1.92(3)	2.696(2)	147(3)	
N2–H2···O4A	0.91(3)	1.93(3)	2.824(3)	171(2)	2–*x*, 1–*y*, 1–*z*
N2A–H2A···O4	0.87(3)	2.02(3)	2.845(3)	158(3)	*x*, 1/2–*y*, 1/2+*z*
O3–H3···O2A	0.98(3)	1.69(3)	2.660(2)	170(3)	2–*x*, –1/2+*y*, 1/2–*z*
O3A–H3A···O2	0.98(3)	1.70(3)	2.676(2)	174(2)	1–*x*, 1/2+*y*, 3/2–*z*
O4A–H4AA···O1	0.87(3)	2.29(3)	3.082(2)	151(3)	*x*, 1/2–*y*, 1/2+*z*
O4–H4A···O1A	0.87(3)	2.25(3)	3.081(2)	160(3)	1–*x*, 1–*y*, 1–*z*
O4–H4B···O2	0.90(2)	1.93(2)	2.817(2)	170(3)	
O4A–H4AB···O2A	0.88(3)	1.94(3)	2.811(3)	169(3)	
H_4L^6					
O1–H1···N1	0.84	1.83	2.570(3)	146	
O1A–H1A···N1A	0.92(6)	1.80(6)	2.573(4)	141(6)	
N2–H2···O2A	0.87(6)	1.88(6)	2.746(3)	173(4)	
N2A–H2A···O2	0.85(6)	1.96(6)	2.796(3)	170(6)	*x*, –1+*y*, *z*
H_4L^7					
O1–H1···N1	0.85(4)	1.88(4)	2.643(3)	150(4)	
O1–H1···O3	0.85(4)	2.56(4)	2.967(3)	111(3)	1–*x*, –1/2+*y*, 3/2–*z*
N2–H2···O1	0.85(4)	2.08(4)	2.922(3)	168(4)	*x*, 1/2–*y*, –1/2+*z*
O3–H3···O2	0.98(5)	1.75(4)	2.678(3)	157(3)	1–*x*, 1/2+*y*, 3/2–*z*

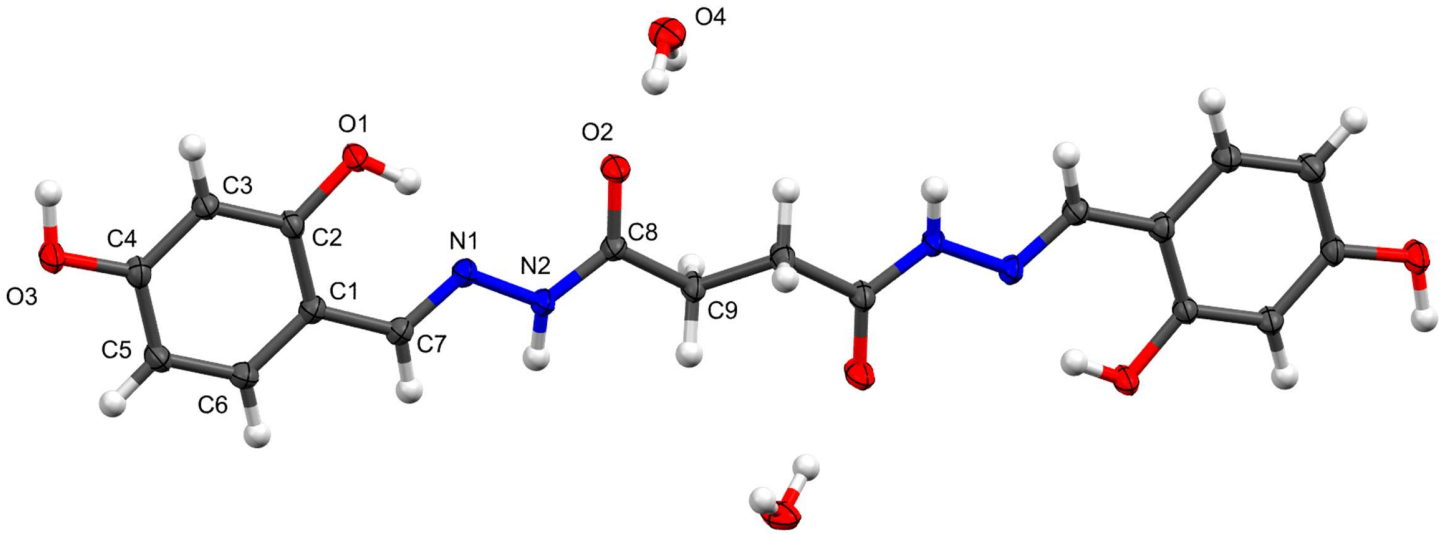

Figure S22. Molecular structure of $\mathbf{H_4L^4 \cdot 2H_2O}$. Molecule is only just non-centrosymmetric, with the whole molecule in the asymmetric unit, along with two water molecules. Atom naming in the right half of the molecule is the same as in the left half of the molecule, with added suffix "A. Aryl fragments are slanted one to the other, with interplanar angle of 5.90°. Distance between aryl ring centroids is 15.8 Å.

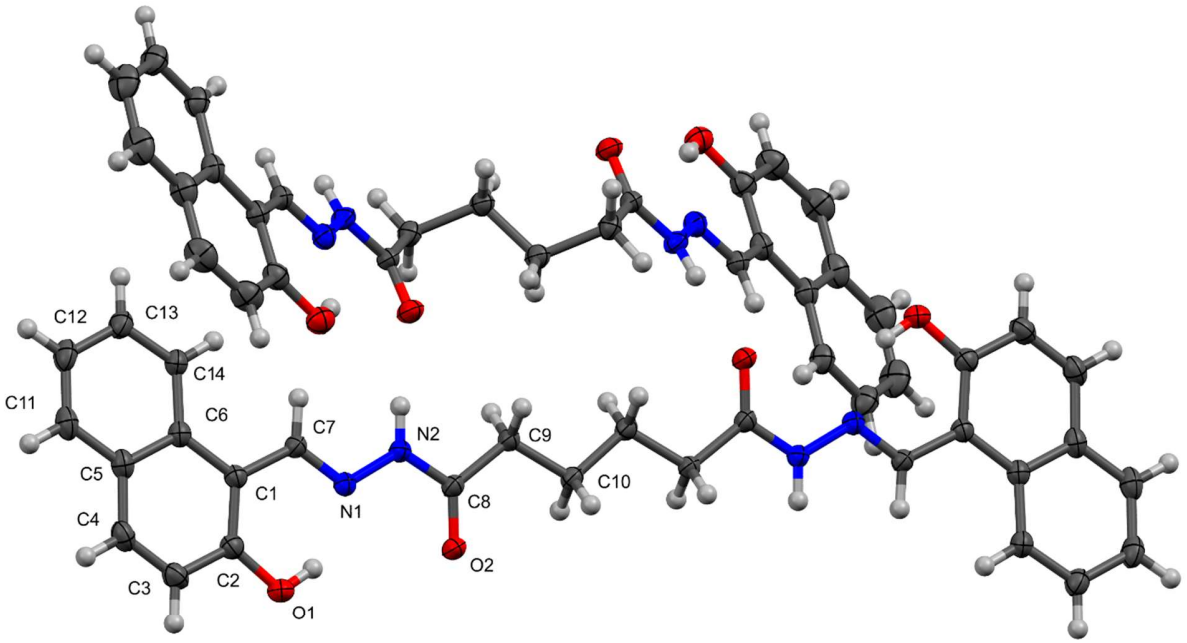

Figure S23. Molecular structure of $\mathbf{H_4L^6}$. Asymmetric unit contains two symmetrically independent molecules. One molecule (bottom) is planar with aryl fragment interplanar distance of 0.683 Å. The other molecule (top) is skewed with aryl fragments interplanar angle of 2°. Planar and skewed molecule have significantly different distances between aryl fragment centroids (16.8 Å vs 19.4 Å).

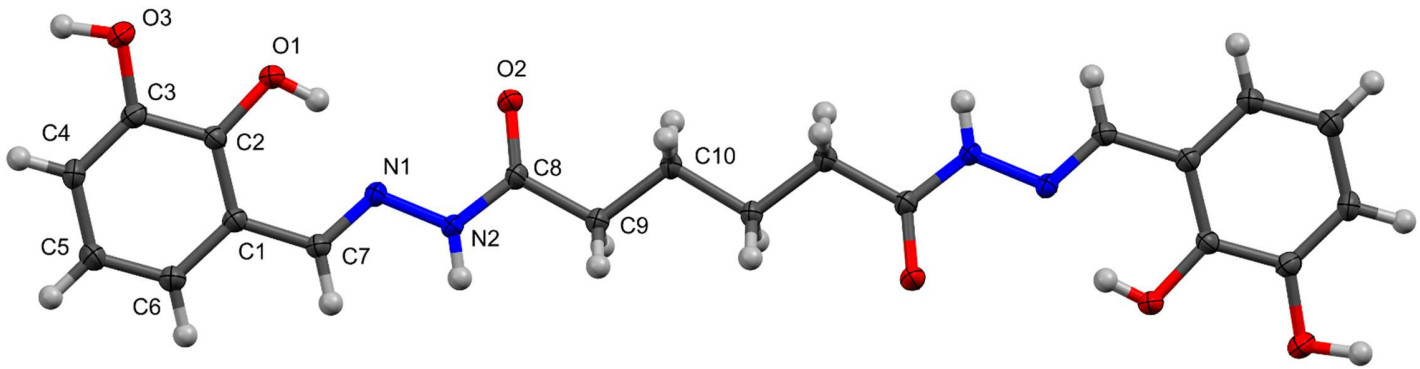

Figure S24. Molecular structure of H_4L^7. Molecule is centrosymmetric with inversion center laying between two central methylene units. Aryl fragments are parallel with interplanar distance of 0.767 Å. Distance between aryl ring centroids is 18.3 Å.

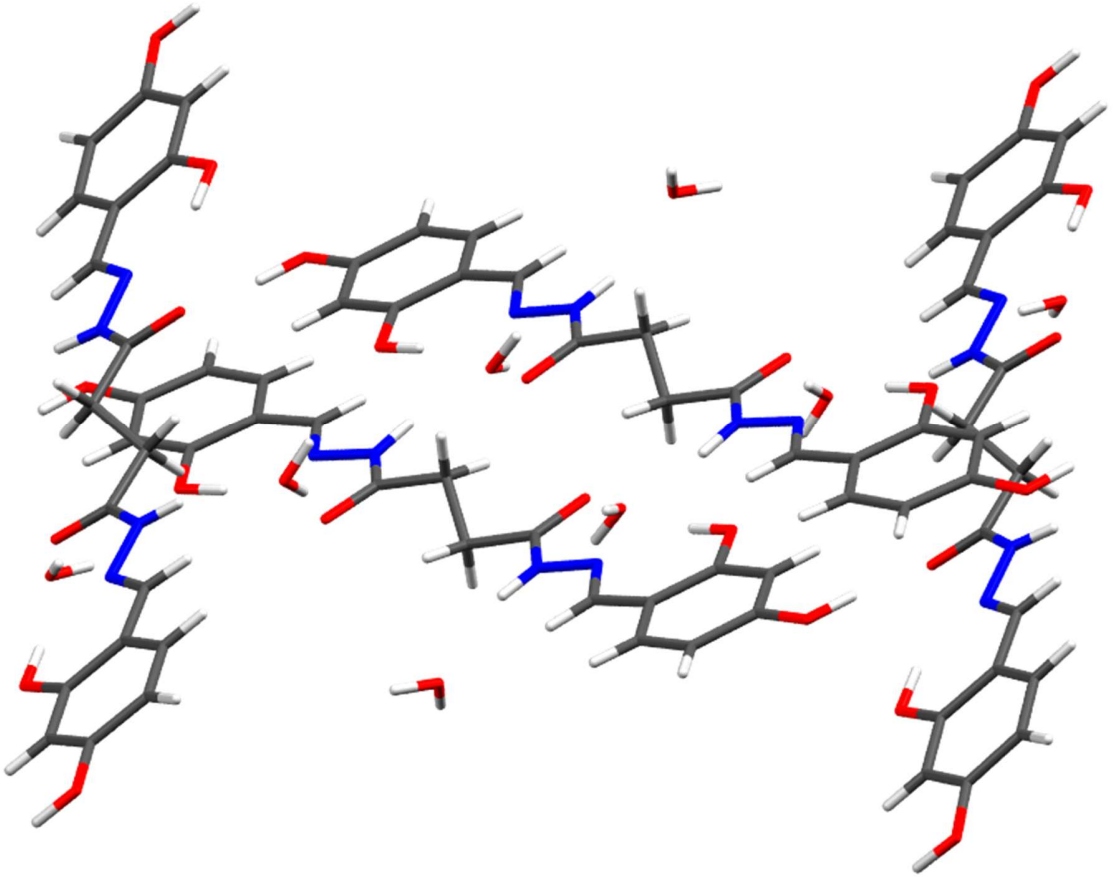

Figure S25. Crystal packing in **$H_4L^4 \cdot 2H_2O$** shown along *a*-axis.

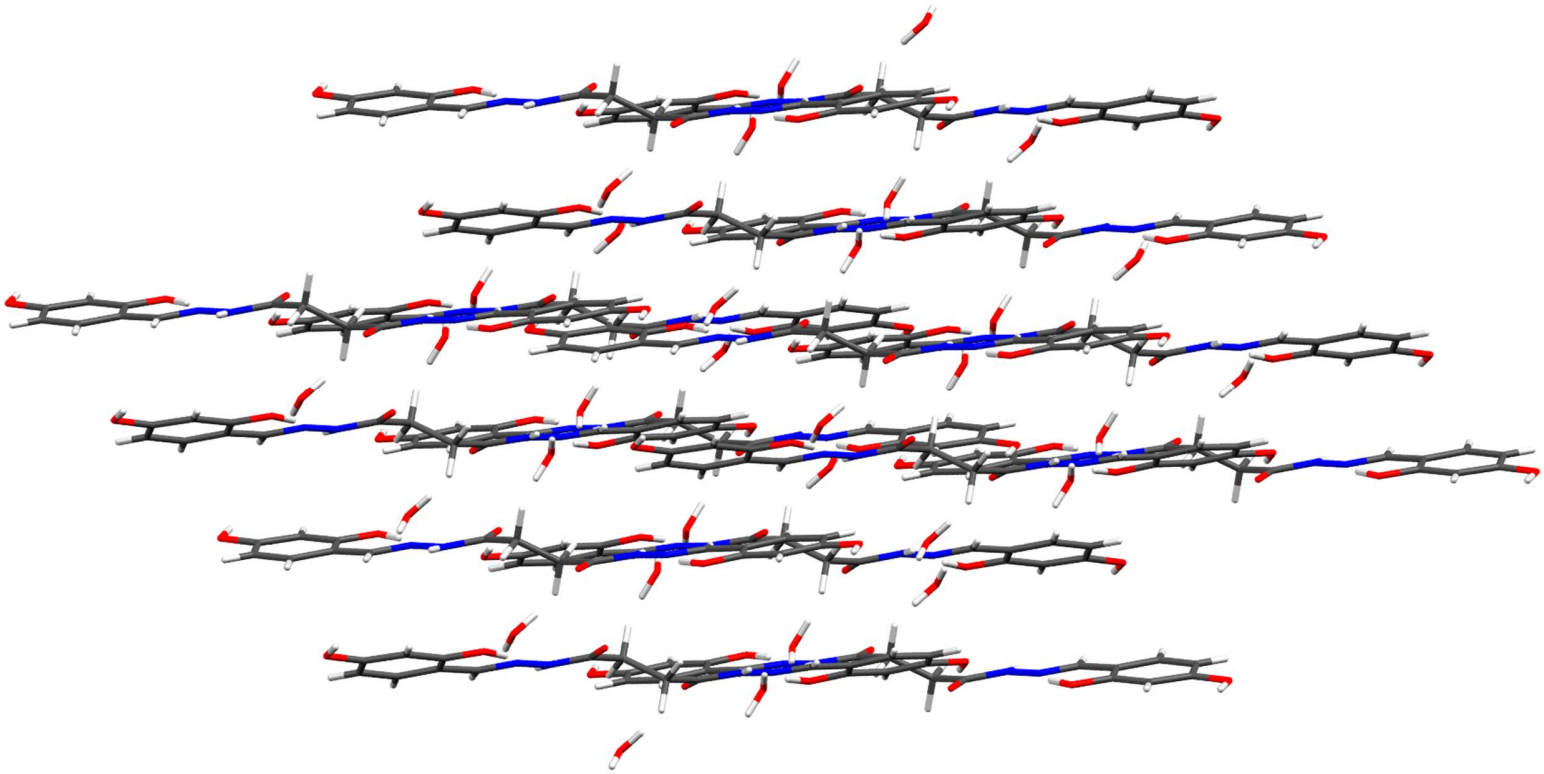

Figure S26. Crystal packing in **$H_4L^4 \cdot 2H_2O$** shown along *a*-axis. Ligand molecules pack in layers bridged by supramolecular interactions with water molecules.

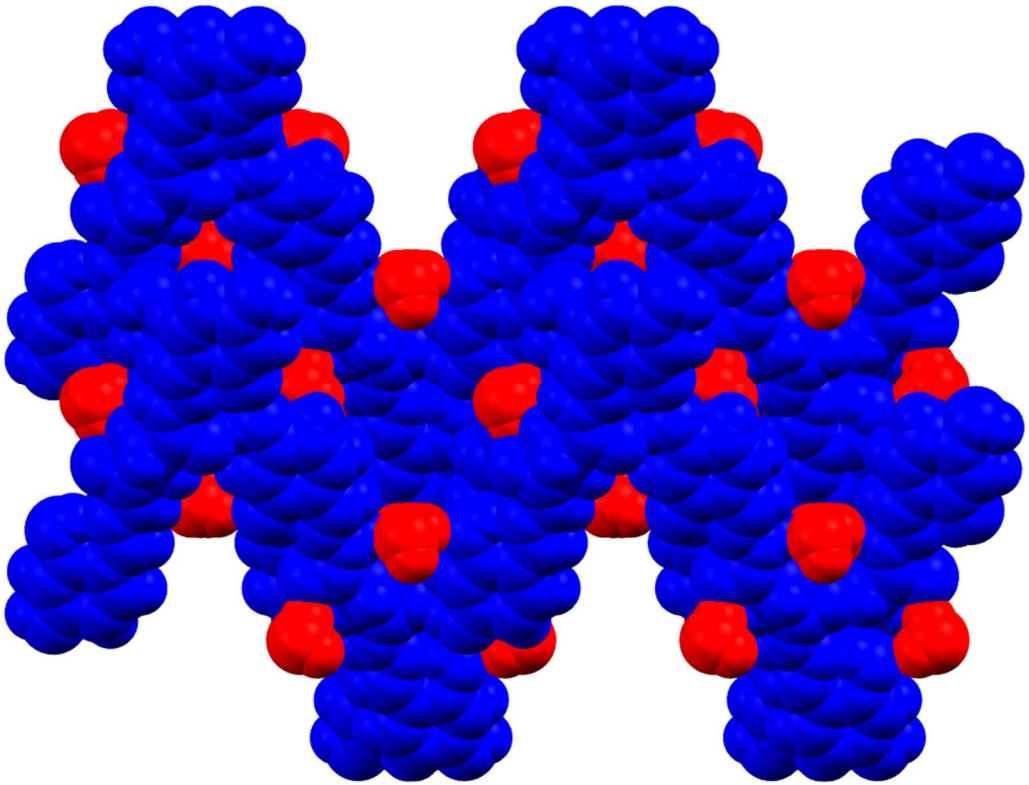

Figure S27. Crystal packing in **$H_4L^4 \cdot 2H_2O$** shown in spacefill style, with blue bodies representing ligand molecules and red bodies representing water molecules.

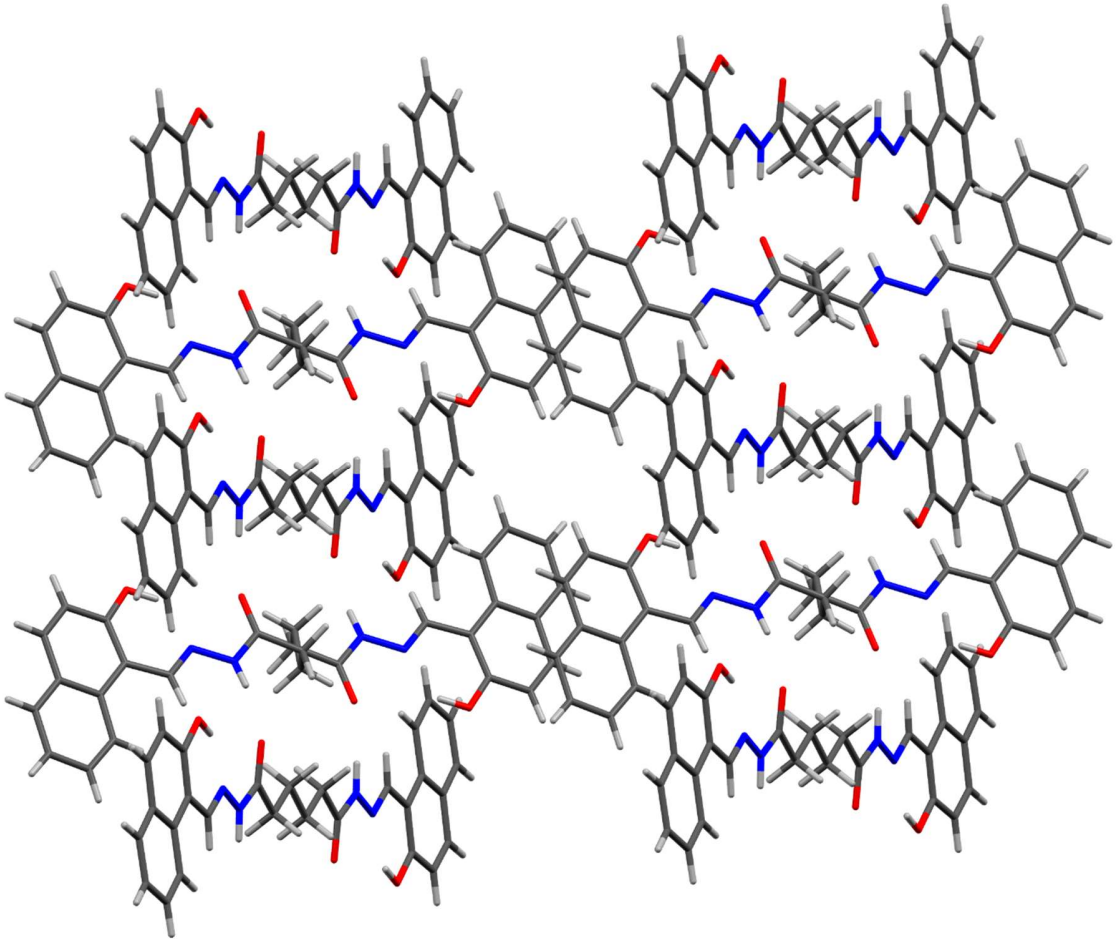

Figure S28. Crystal packing in **H_4L^6** shown along *a*-axis.

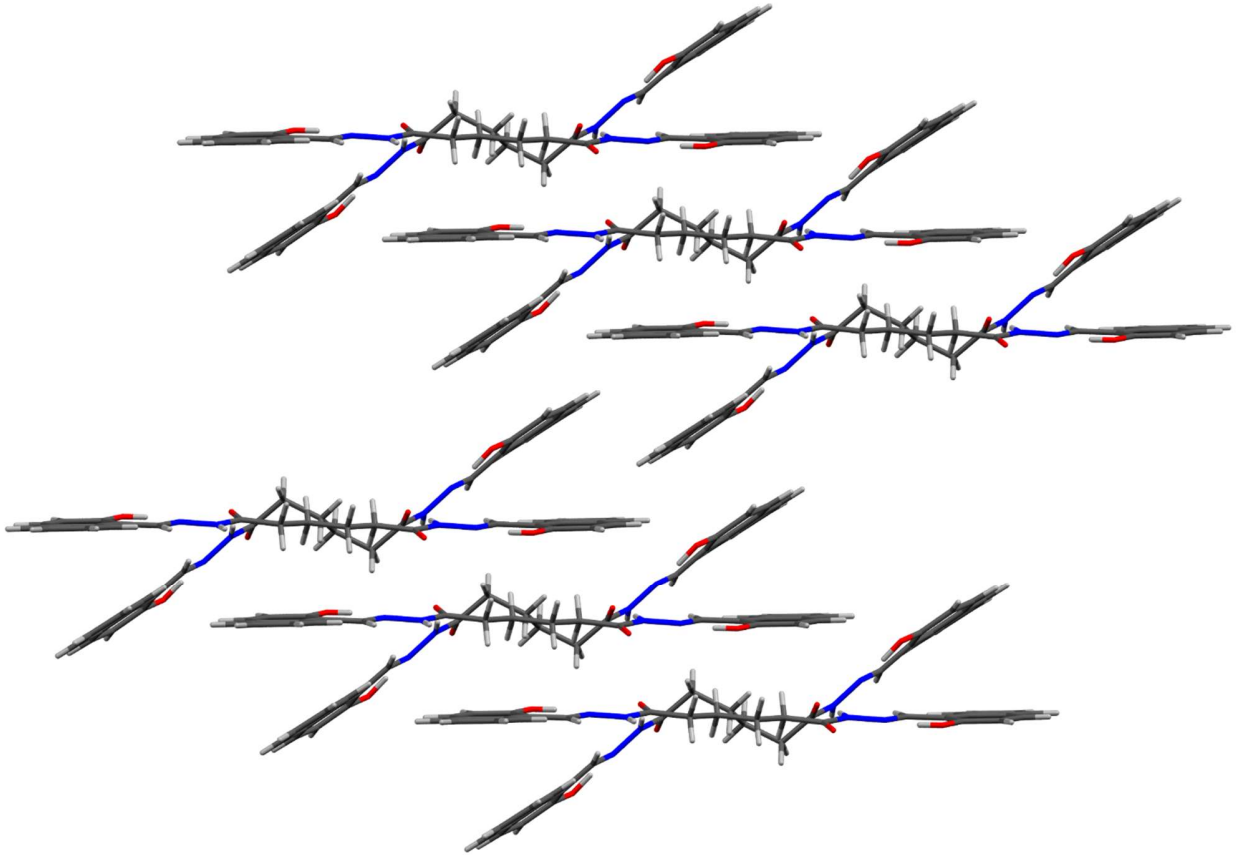

Figure S29. Crystal packing in **H_4L^6** shown along *b*-axis, showing a clear contrast in geometry between two symmetrically independent ligand molecules.

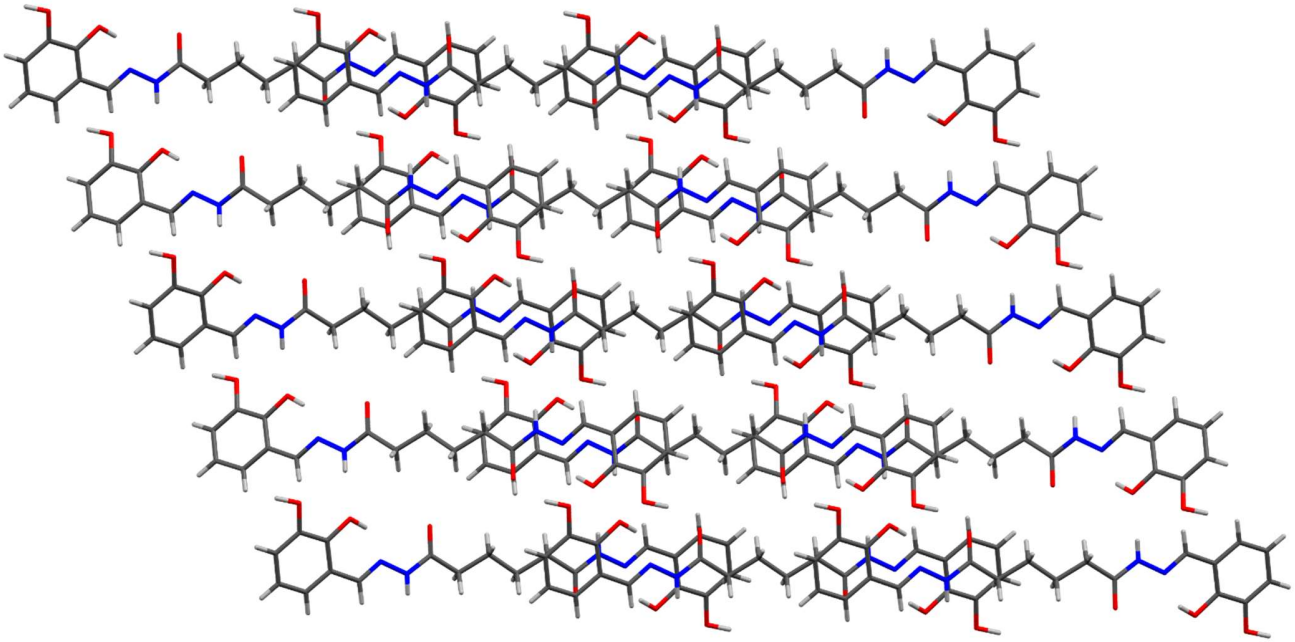

Figure S30. Crystal packing in $\mathbf{H_4L^7}$ shown along *b*-axis.

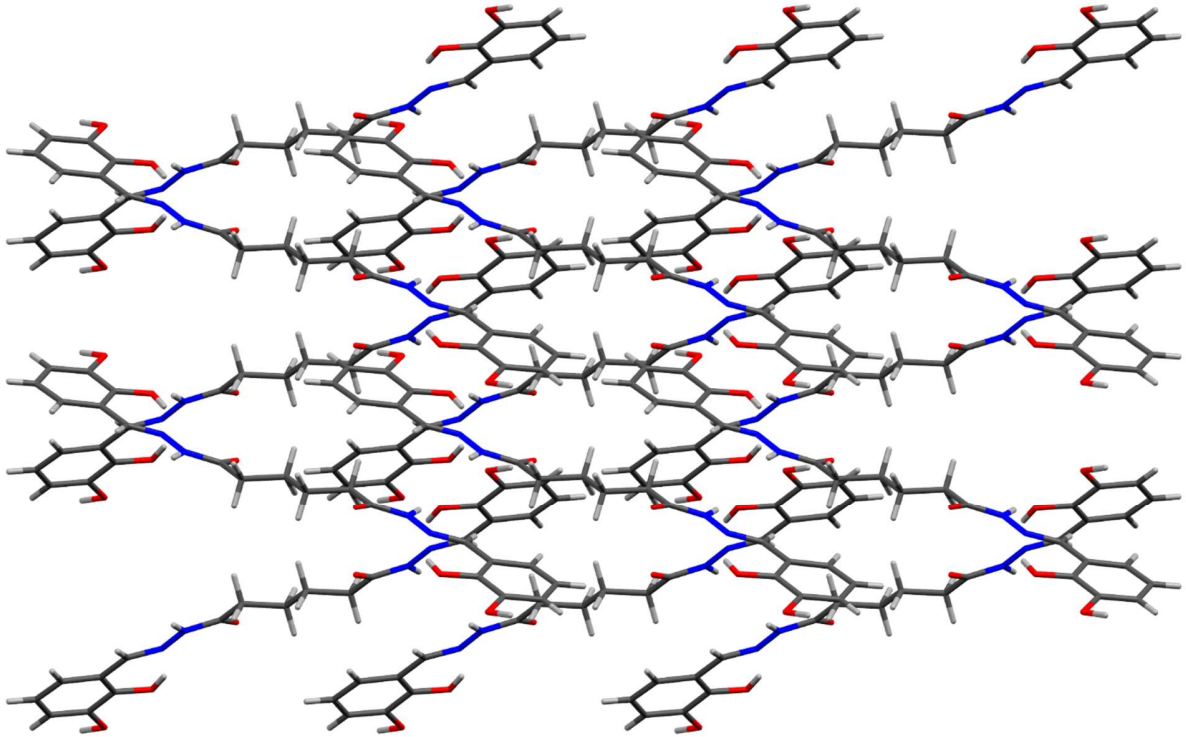

Figure S31. Crystal packing in $\mathbf{H_4L^7}$ shown along *c*-axis.

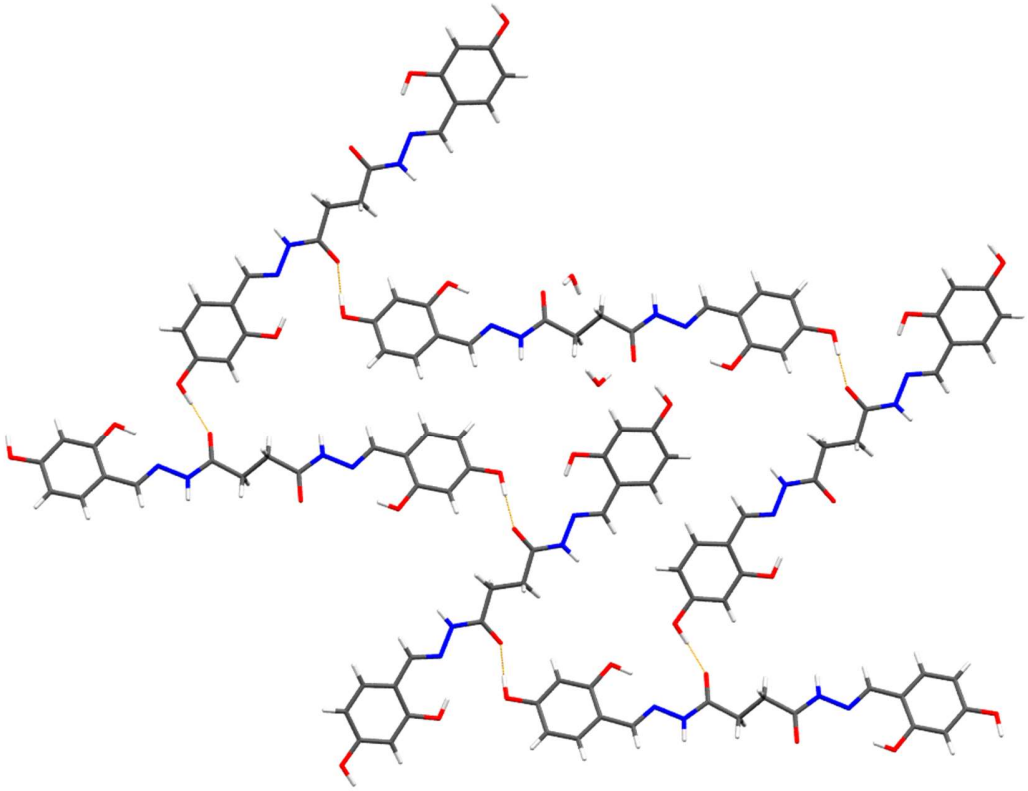

Figure S32. Intralayer hydrogen bond network in the crystal structure of **$H_4L^4 \cdot 2H_2O$**, built from aryl-OH···O=C hydrogen bonds, forming a supramolecular ring $R_6^6(78)$.

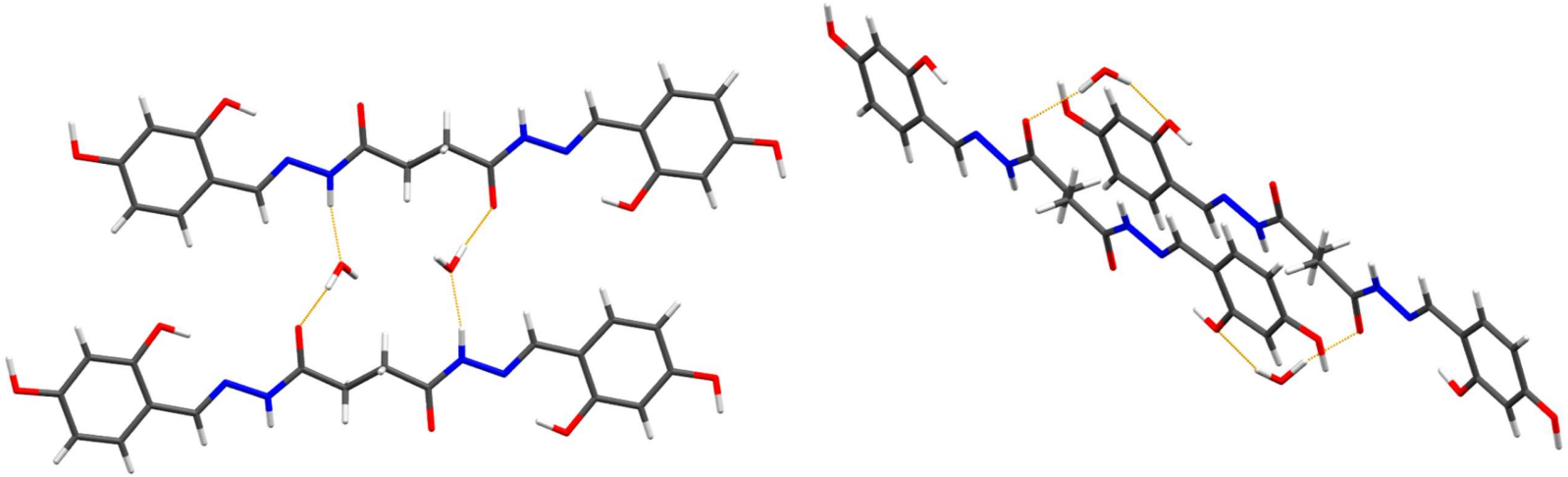

(a) (b)

Figure S33. Examples of interlayer hydrogen bond interactions in **$H_4L^4 \cdot 2H_2O$**, which are established through water molecules, again employing amido carbonyl as hydrogen bond acceptor. Water serves as ditopic or tritopic hydrogen bond donor and acceptor.

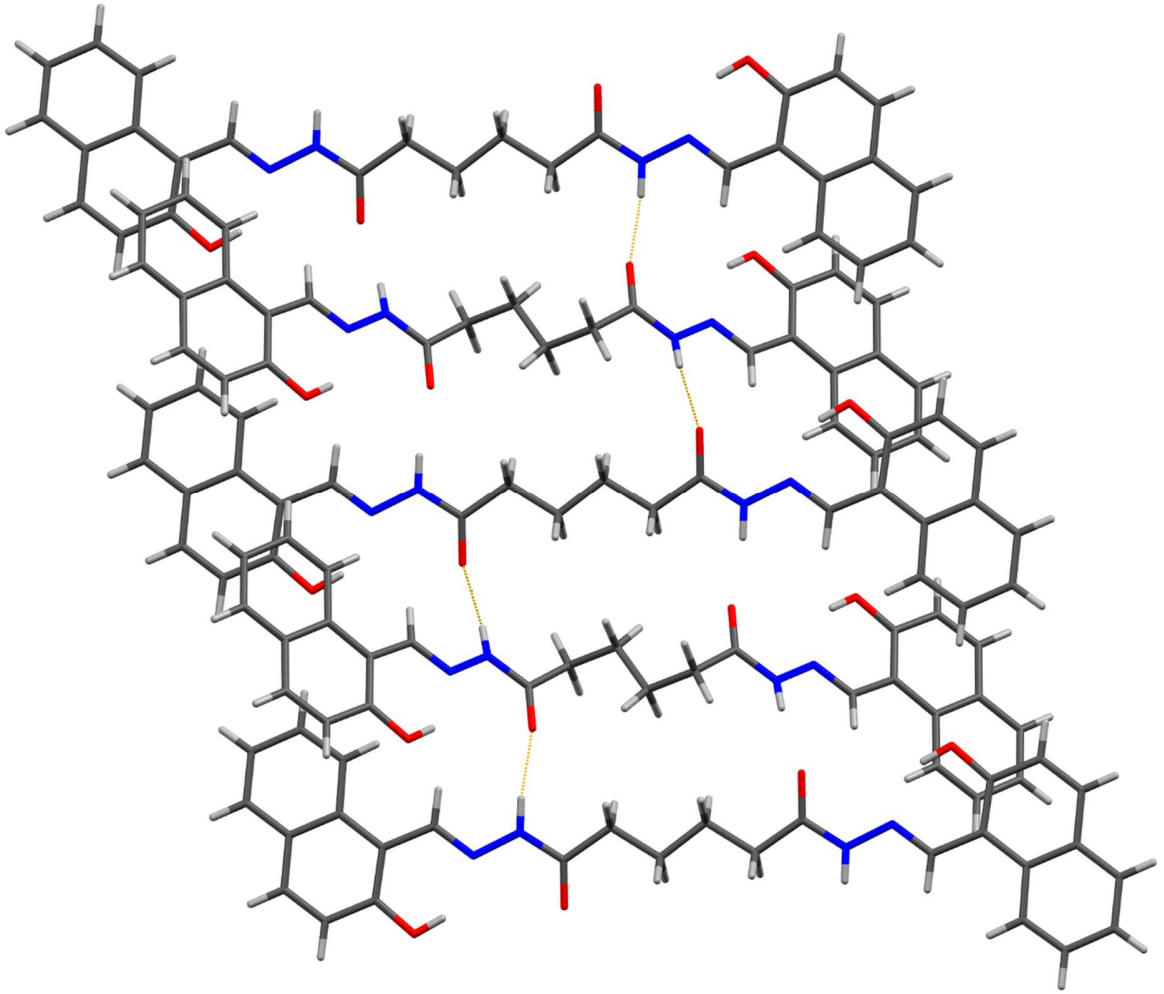

Figure S34. Supramolecular chain $C_4^4(26)$ connecting the two symmetrically independent molecules of **H_4L^6**. The molecules are connected through amide hydrogen bond motif.

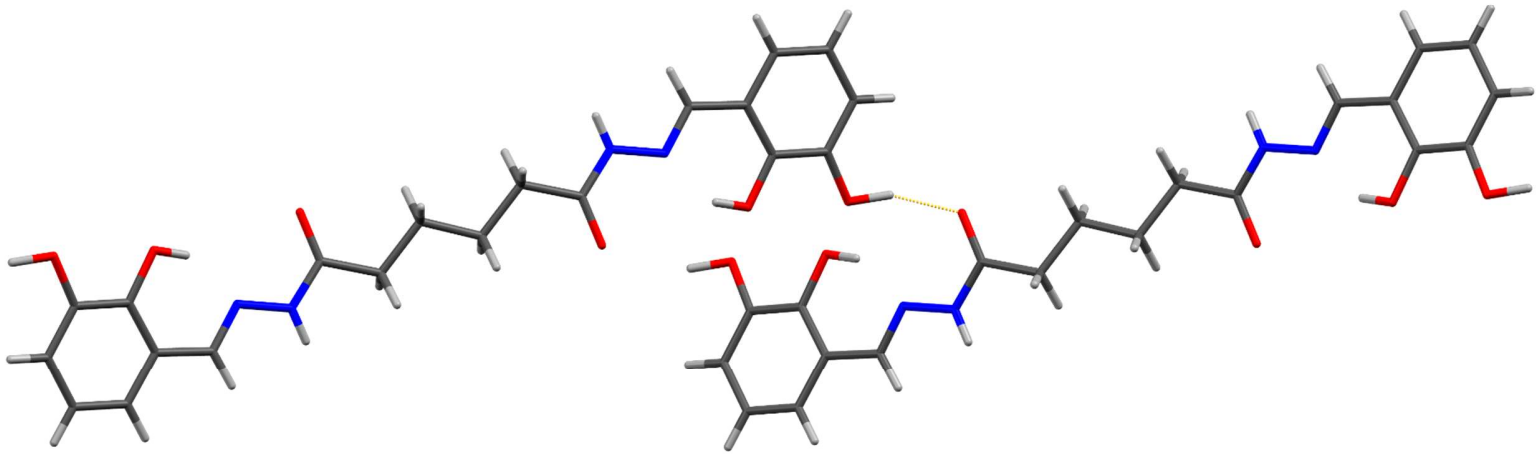

Figure S35. Supramolecular chain $C_1^1(10)$ connecting the two molecules of **H$_4$L^7**. The molecules are connected through 3-hydroxyaryl-amide carbonyl hydrogen bond.

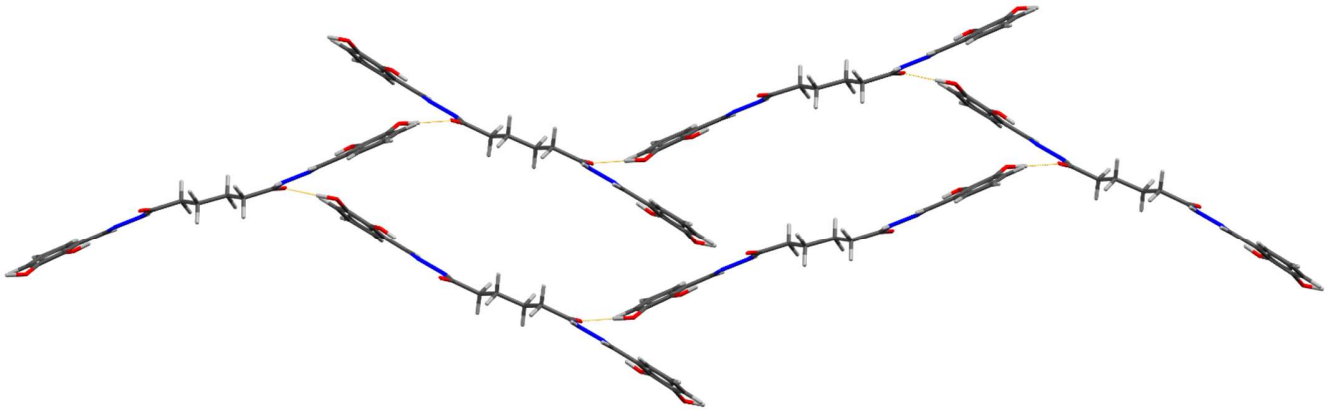

Figure S36. Supramolecular ring $R_8^8(60)$ connecting the six molecules of **H$_4$L^7**.

NMR spectroscopy

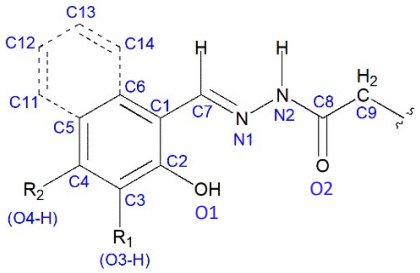

(a)

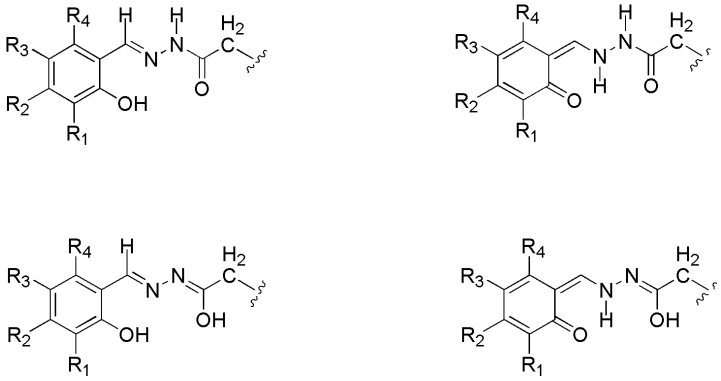

(b)

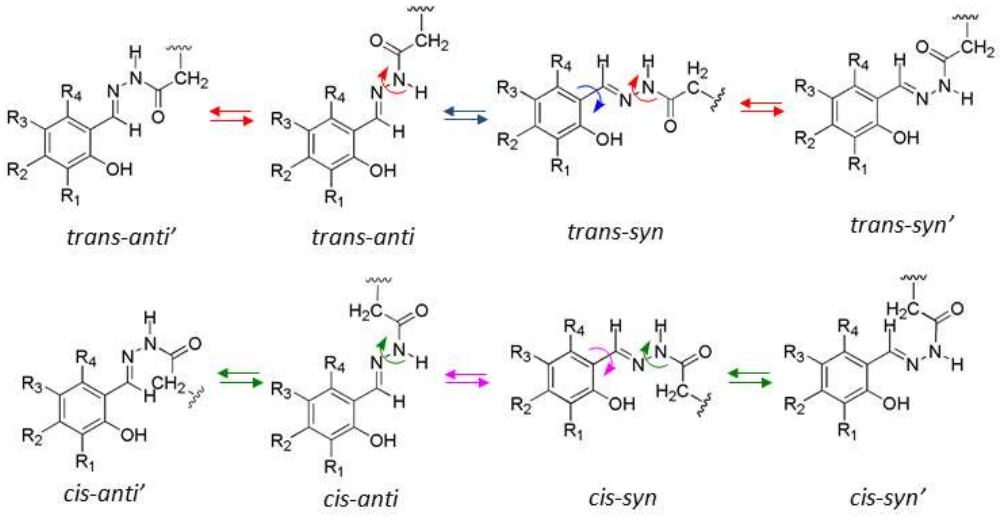

(c)

Scheme S2. (a) Atom numbering scheme for subunit of H_4L^1-H_4L^4; (b) four possible tautomeric forms in which subunits of H_4L^1-H_4L^4 can exist; (b) possible conformations of subunits (shown for the established enol-imino tautomeric form) for compounds H_4L^1-H_4L^4 in DMSO solution. In (b) *cis*/*trans* isomerisation corresponds to rotation around the -(C=O)–NH- hydrazone linkage. R_1, R_2 = H, OH; R_3, R_4 = $(CH)_4$.

Table S5. Partial ^{1}H, ^{13}C and ^{15}N assignment for the investigated compounds (**H_4L^1-H_4L^4**) in DMSO-d_6 at 25 °C. ^{15}N chemical shifts are reported relative to liquid ammonia.

Atoms[a]		H_4L^1			H_4L^2			H_4L^3				H_4L^4	
	δ_H, ppm	δ_C, ppm	δ_N, ppm	δ_H, ppm	δ_C, ppm	δ_N, ppm	δ_H, ppm	δ_C, ppm	δ_N, ppm	δ_H, ppm	δ_C, ppm	δ_N, ppm
2		157.7 156.7			158.2			145.6 146.4			158.6 159.8 160.7 161.0	
7	8.28 8.29 8.35	141.4[b] 141.5[b] 146.7[b] 146.9[b]		8.96 8.93 9.16 9.18	142.7[b] 142.8[b] 145.1[b] 145.2[b] 145.3[b]		8.26 8.27 8.31	142.4[b] 142.5[b] 147.6[b]		8.13 8.14 8.21	142.8[b] 147.7[b] 147.8[b]	
8		168.1 168.4 173.4 173.5			167.9			168.0 168.3 173.2 173.4			167.7 167.9 172.8 173.0	
O1; O3; O4	10.13 10.14 11.17 11.21; -; -			11.14 11.18 12.59 12.61 12.63; -; -			11.01 11.06 9.43[d] 9.45[d] 9.48[d] 9.53[d]; 9.16 9.17			9.89[e] 10.15[e] 11.35[e]		
N1			302.5 312.0			296.3 307.7			301 310			291 300
N2	11.28 11.29 11.70 11.72		174.0[c] 179.2[c]	11.30 11.38 11.76 11.83 11.85		173.4[c] 179.6[c]	11.30 11.31 11.70 11.72		172.4[c] 179.0[c]	11.09 11.10 11.48 11.51		172.0[c] 177.8[c]

[a] For atom numbering scheme, see Scheme S2.
[b] Assignment based on ^{1}H-^{13}C HSQC spectrum.
[c] Assignment based on ^{1}H-^{15}N HSQC spectrum.
[d] Signals of O1–H and O3–H could not be unambiguously distinguished.
[e] Signals of O1–H and O4–H could not be unambiguously distinguished.

Signals belonging to $–CH_2–CH_2–$ bridges appear in well expected range, *ca.* 2.5–3 ppm (^{1}H NMR) and ≈ 27–29 ppm (^{13}C NMR). The remaining signals arising from aromatic C and H atoms of the aldehyde residues are found at the expected ranges.

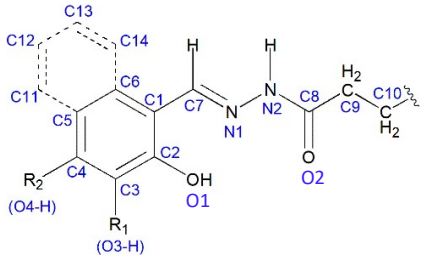

(a)

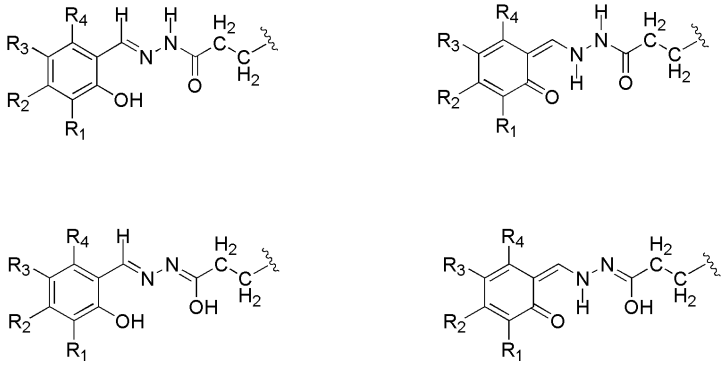

(b)

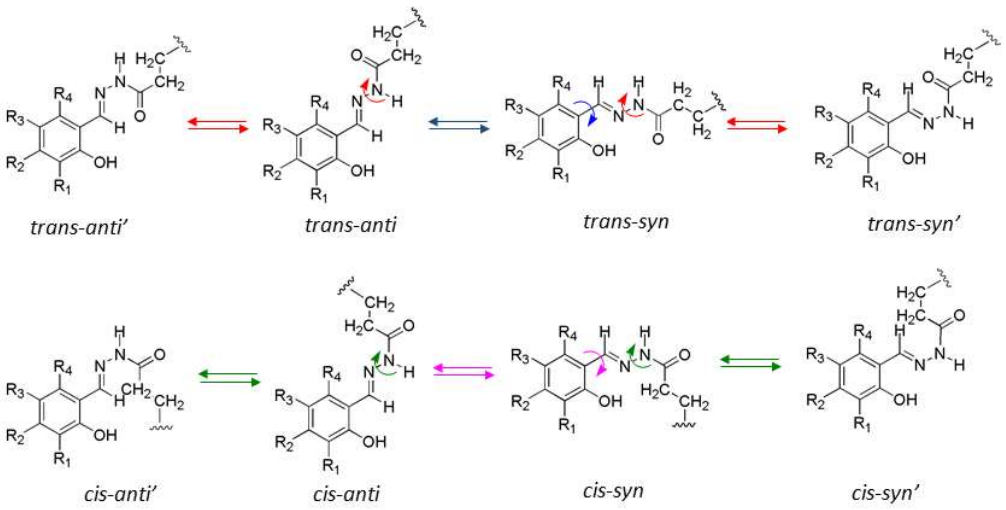

(c)

Scheme S3. (a) Atom numbering scheme for subunit of $\mathbf{H_4L^5}$-$\mathbf{H_4L^8}$; (b) four possible tautomeric forms in which subunits of $\mathbf{H_4L^5}$-$\mathbf{H_4L^8}$ can exist; (b) possible conformations of subunits (shown only for enol-imino/keto-amino tautomeric form) for compounds $\mathbf{H_4L^5}$-$\mathbf{H_4L^8}$ in DMSO solution. In (b) cis/trans isomerisation corresponds to rotation around the -(C=O)–NH- hydrazone linkage. R_1, R_2 = H, OH; R_3, R_4 = $(CH)_4$.

Table S6. Partial ^{1}H, ^{13}C and ^{15}N assignment for the investigated compounds (**H_4L^5- H_4L^8**) in DMSO-d_6 at 25 °C. ^{15}N chemical shifts are reported relative to liquid ammonia.

Atoms[a]		H_4L^5			H_4L^6			H_4L^7			H_4L^8	
	δ_H, ppm	δ_C, ppm	δ_N, ppm	δ_H, ppm	δ_C, ppm	δ_N, ppm	δ_H, ppm	δ_C, ppm	δ_N, ppm	δ_H, ppm	δ_C, ppm	δ_N, ppm
2		156.8 157.8			158.6 157.3			145.9 146.4 145.6			158.5 159.8 161.0 160.7	
7	8.27 8.35	141.2[b] 147.0[b]		8.94 8.93 9.12 9.17	142.7[b] 145.4[b]		8.25 8.30	142.2[b] 147.8[b]		8.13 8.22	142.6[b] 147.9[b]	
8		168.7 174.2 174.1			168.6 173.7			168.7 177.0 174.1			168.4 173.7	
O1	10.13 11.20			≈12.6				9.43[d] 9.44[d] 9.46[d] 11.07[d] 11.08[d] 11.22[d]		≈10[e] ≈11[e]		
N1			303.0 312.7			296.1 308.1			300.9 311.3			291.5 300.8
N2	11.22 11.58 11.60		174.4[c] 180.6[c]	≈11.3 ≈11.7		174.3[c] 180.6[c]	11.23 11.61		174.5[c] 179.9[c]	11.03 11.40 11.43		173.4[c] 178.4[c]

[a] For atom numbering scheme, see Scheme S3.
[b] Assignment based on ^{1}H-^{13}C HSQC spectrum.
[c] Assignment based on ^{1}H-^{15}N HSQC spectrum.
[d] Signals of O1–H and O3–H could not be unambiguously distinguished.
[e] Signals of O1–H and O4–H could not be unambiguously distinguished.

Signals belonging to $–CH_2–CH_2–$ $CH_2–CH_2–$ bridges appear in well expected range, *ca.* 2.5–3 ppm (^{1}H NMR) and ≈ 27–29 ppm (^{13}C NMR). The remaining signals arising from aromatic C and H atoms of the aldehyde residues are found at the expected ranges.

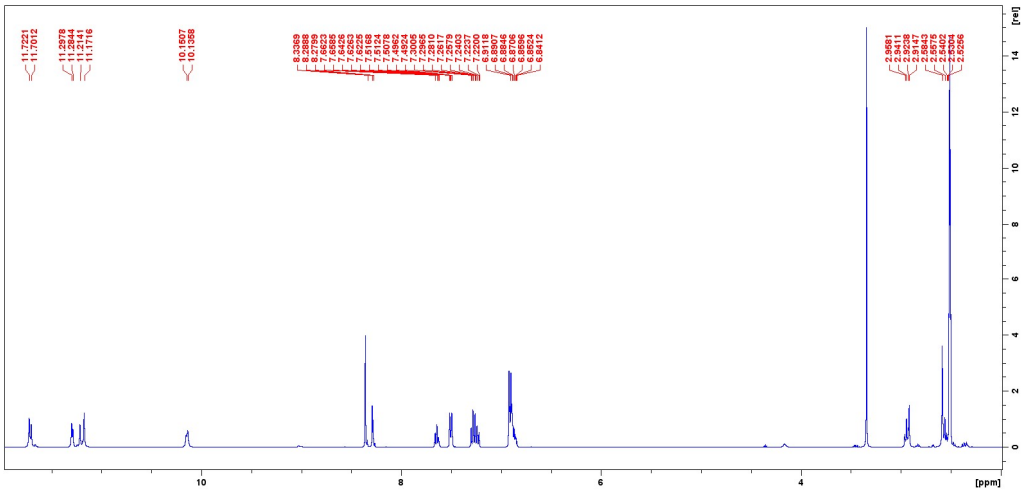
11.7221
11.7012
11.2978
11.2844
11.2644
11.1716
10.1607
10.1398
8.3388
8.3088
8.2799
7.6623
7.6468
7.6426
7.6253
7.6168
7.5974
7.5078
7.4962
7.4804
7.3005
7.2965
7.2810
7.2617
7.2573
7.2450
7.2237
7.2010
6.9119
6.8907
6.8896
6.8706
6.8596
6.8504
6.8412
3.9681
3.9411
3.9268
2.9147
2.8973
2.8673
2.8543
2.5402
2.5284
2.5296
[rel]
[ppm]

(a)

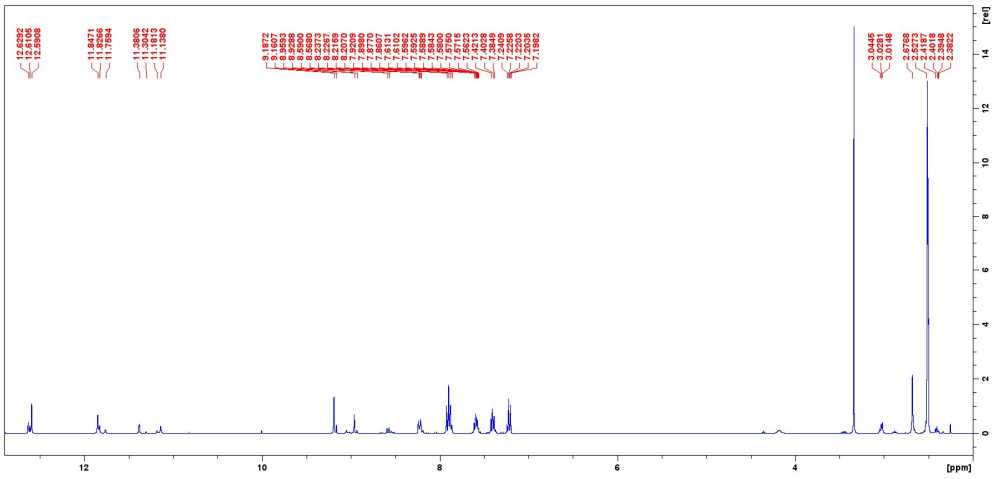
12.6292
12.6106
12.5988
11.8471
11.8268
11.7084
11.3806
11.3042
11.1983
11.1889
9.1677
9.1507
8.9593
8.9388
8.8980
8.8693
8.8370
8.2267
8.2179
8.2070
7.9209
7.8969
7.8770
7.8607
7.8511
7.6102
7.5952
7.5925
7.5889
7.5843
7.5800
7.5719
7.5715
7.5623
7.4513
7.4023
7.3849
7.3469
7.2298
7.2203
7.2035
7.1982
3.0445
3.0251
3.0148
2.6768
2.5273
2.5187
2.4918
2.3848
2.3622
[rel]
[ppm]

(b)

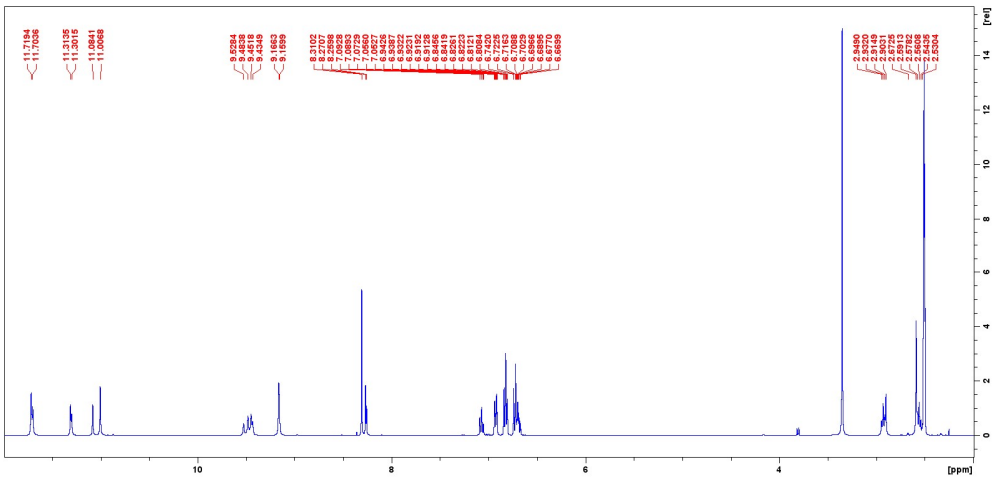
11.7194
11.7036
11.3135
11.3015
11.0841
11.0068
9.5284
9.4838
9.4658
9.4348
9.1663
9.1699
8.3102
8.2770
8.2286
7.0828
7.0688
7.0729
7.0660
7.0562
6.9426
6.9231
6.9052
6.9128
6.8946
6.8843
6.8261
6.8223
6.8121
6.8084
6.7940
6.7225
6.7163
6.7088
6.7029
6.6966
6.6896
6.6770
6.6669
2.9480
2.9300
2.9149
2.8731
2.8591
2.5913
2.5782
2.5606
2.5435
2.5304
[rel]
[ppm]

(c)

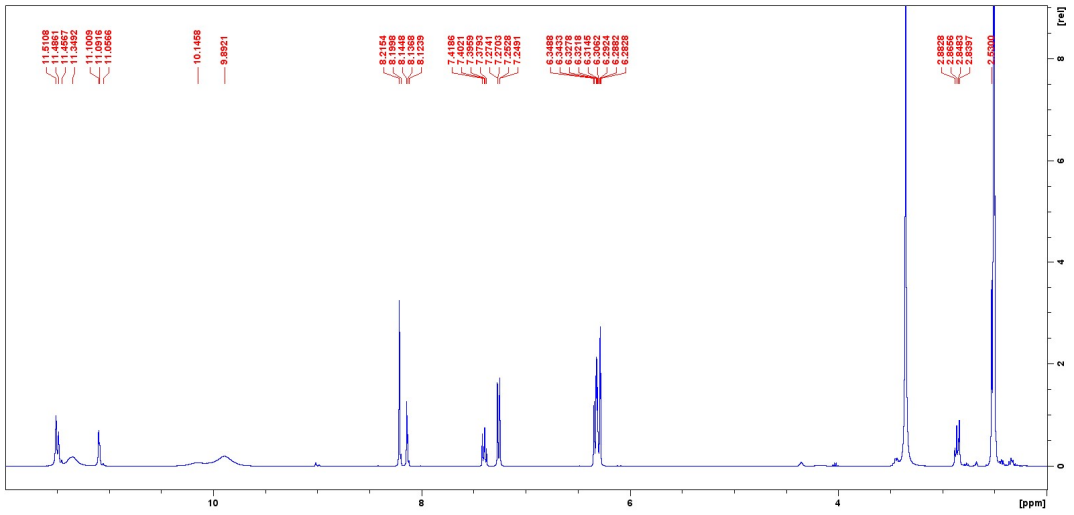

(d)

Figure S37. ^{1H} NMR spectra of a) $\mathbf{H_4L^1}$; b) $\mathbf{H_4L^2}$; c) $\mathbf{H_4L^3}$ and d) $\mathbf{H_4L^4}$ in DMSO-d_6, at 25 °C.

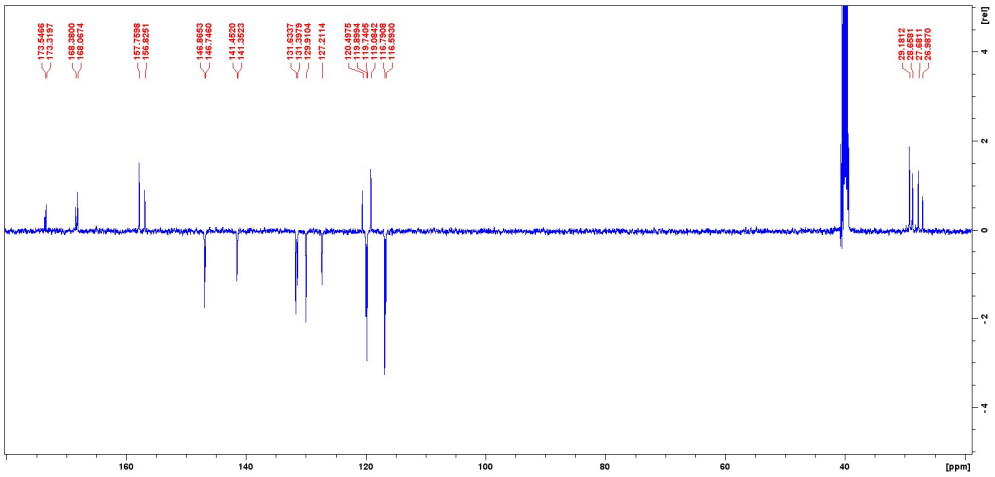
173.5466
173.3197
168.3800
168.0674
157.7598
156.8251
146.8653
146.7460
141.4520
141.3523
131.6337
131.3979
129.9104
127.2114
120.4975
119.8994
119.7405
119.0842
116.7908
116.5930
29.1812
28.6881
27.6811
26.9870
[rel]
[ppm]

(a)

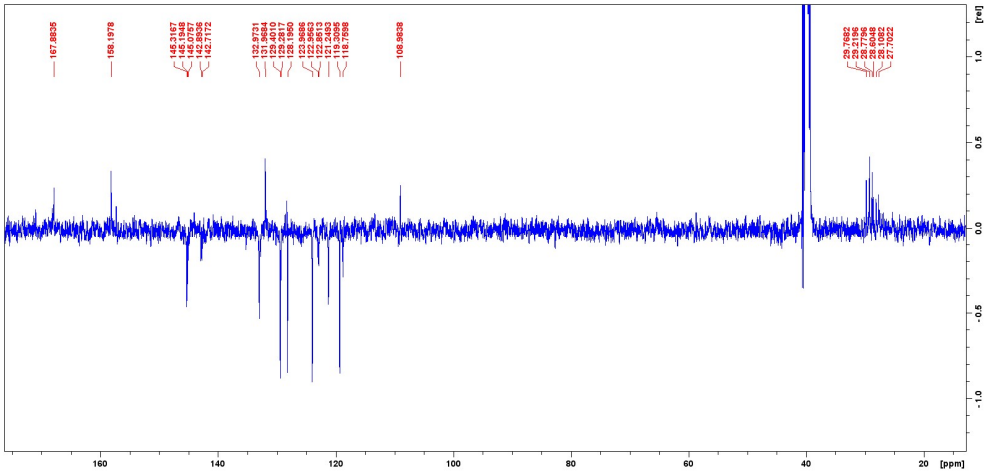
167.8835
158.1978
145.3167
145.1948
145.0757
142.8936
142.7172
132.9731
131.9684
129.4010
129.2817
128.1950
123.9686
122.9563
122.8513
121.2493
119.3095
118.7598
108.9838
29.7682
29.2196
28.7796
28.6048
28.1082
27.7022
[rel]
[ppm]

(b)

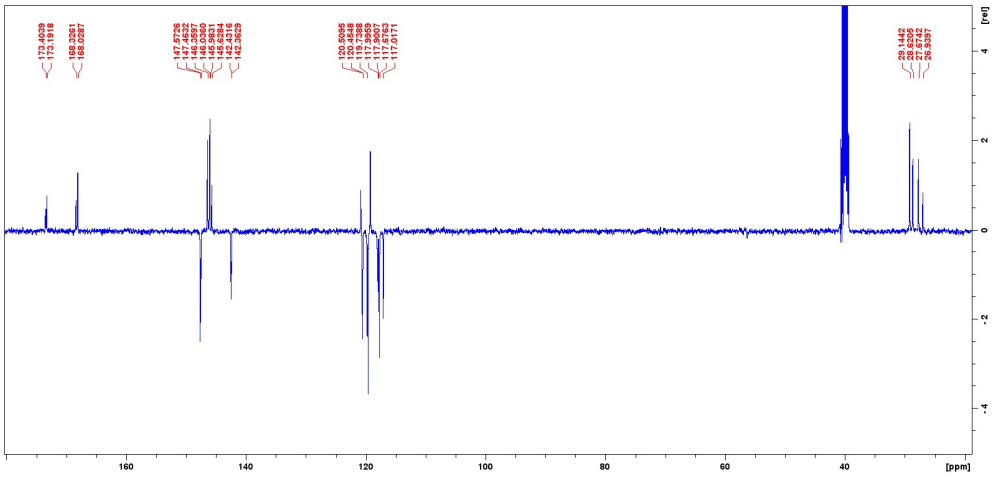
173.4039
173.1918
168.3261
168.0287
147.5726
147.4632
146.3597
146.0360
145.9831
145.6284
142.4316
142.3629
120.5095
120.4548
119.7388
117.9959
117.9007
117.6763
117.0171
29.1442
28.6205
27.6742
26.9397
[rel]
[ppm]

(c)

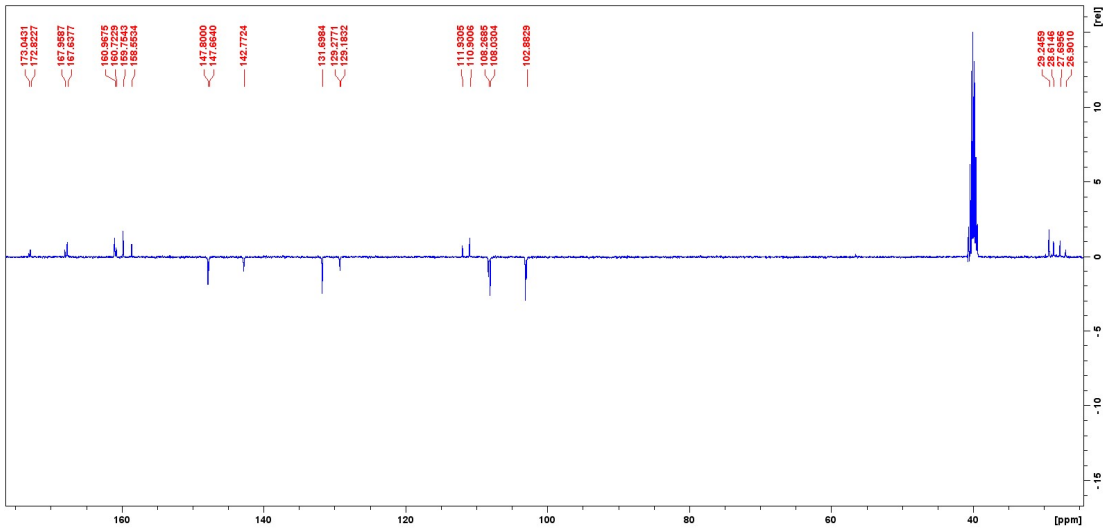

(d)

Figure S38. ^{13}C NMR spectra of a) $\mathbf{H_4L^1}$; b) $\mathbf{H_4L^2}$; c) $\mathbf{H_4L^3}$ and d) $\mathbf{H_4L^4}$ in DMSO-d_6, at 25 °C.

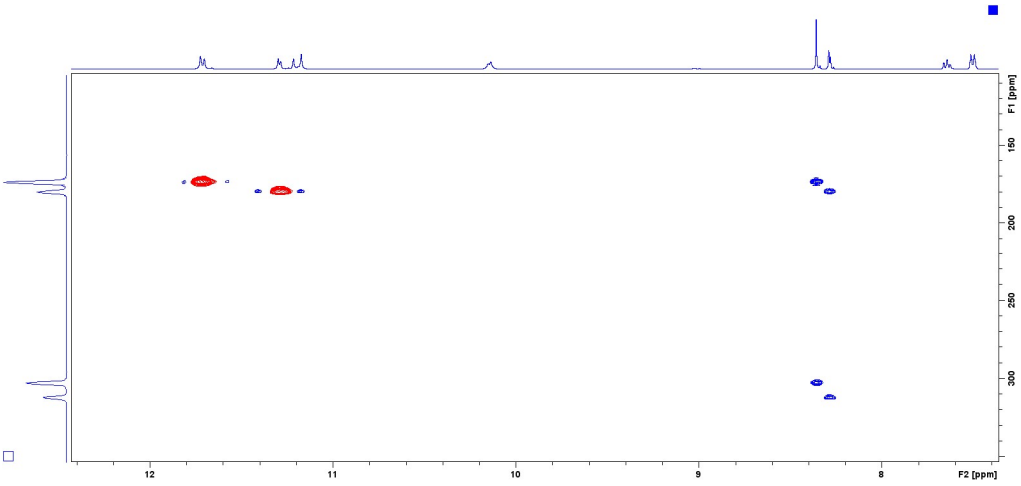
F1 [ppm]
150
200
250
300
12
11
10
9
8
F2 [ppm]

(a)

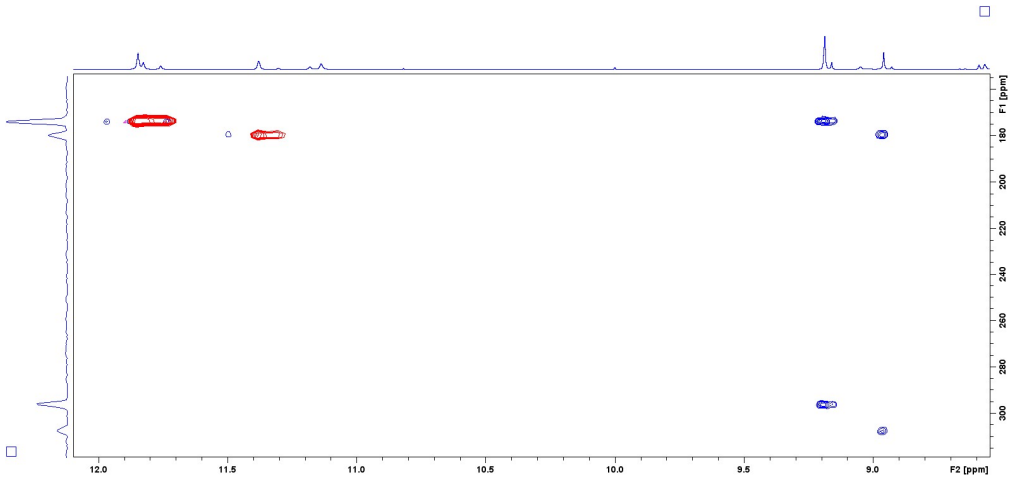
F1 [ppm]
180
200
220
240
260
280
300
12.0
11.5
11.0
10.5
10.0
9.5
9.0
F2 [ppm]

(b)

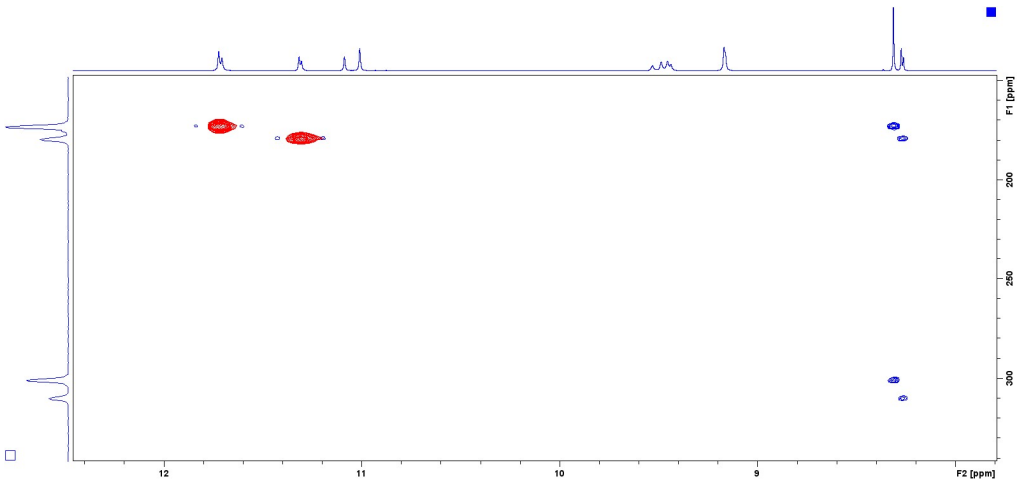
F1 [ppm]
200
250
300
12
11
10
9
F2 [ppm]

(c)

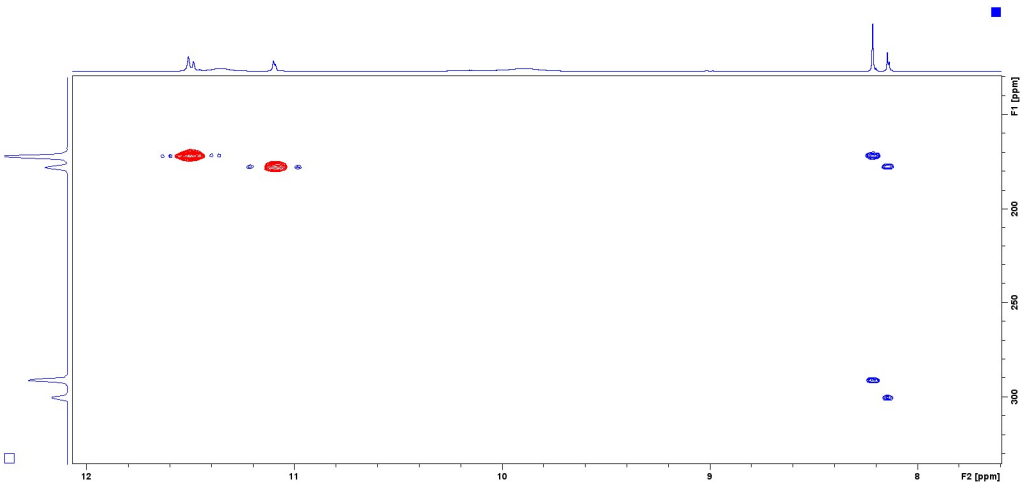

(d)

Figure S39. ^{1}H-^{15}N HSQC-HMBC overlay of spectra for a) $\mathbf{H_4L^1}$; b) $\mathbf{H_4L^2}$; c) $\mathbf{H_4L^3}$ and d) $\mathbf{H_4L^4}$ in DMSO-d_6, at 25 °C. In all cases ^{1}H-^{15}N HSQC signals are shown in red, whereas ^{1}H-^{15}N HMBC signals are shown in blue.

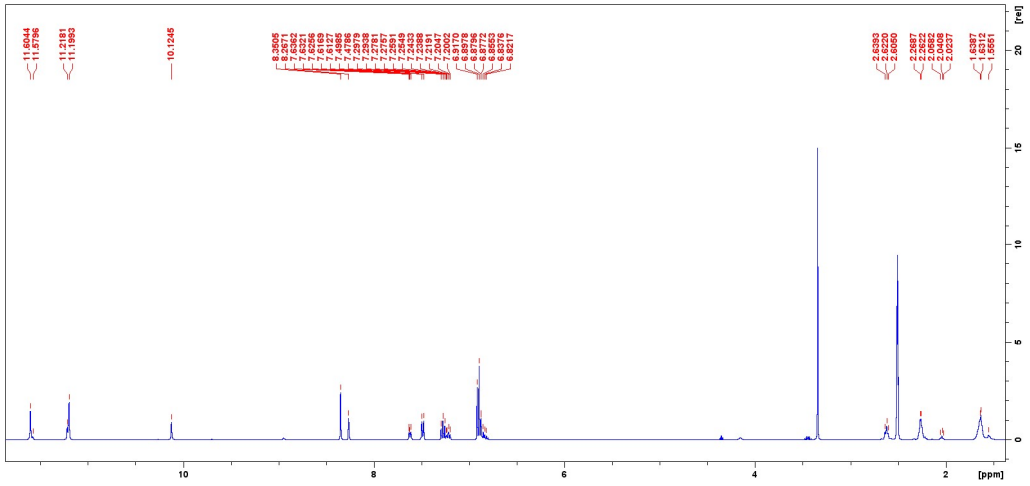

(a)

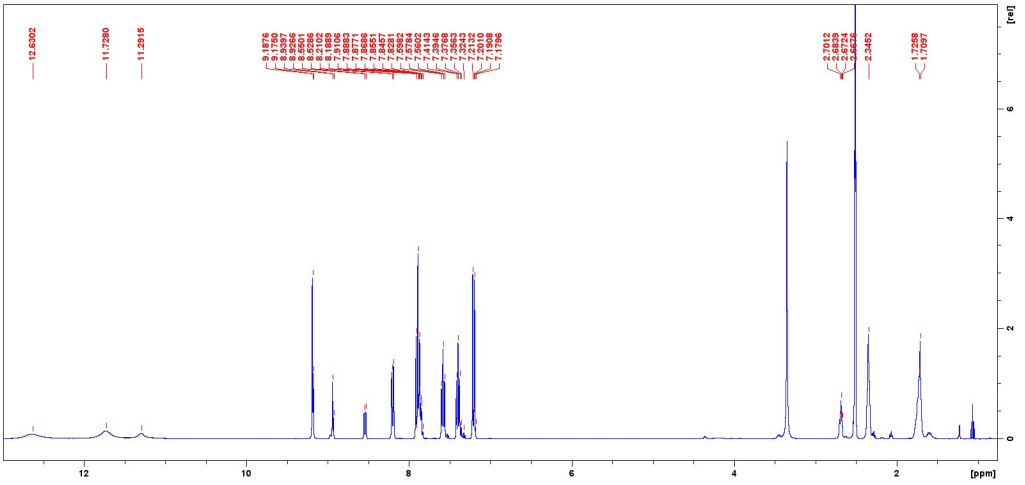

(b)

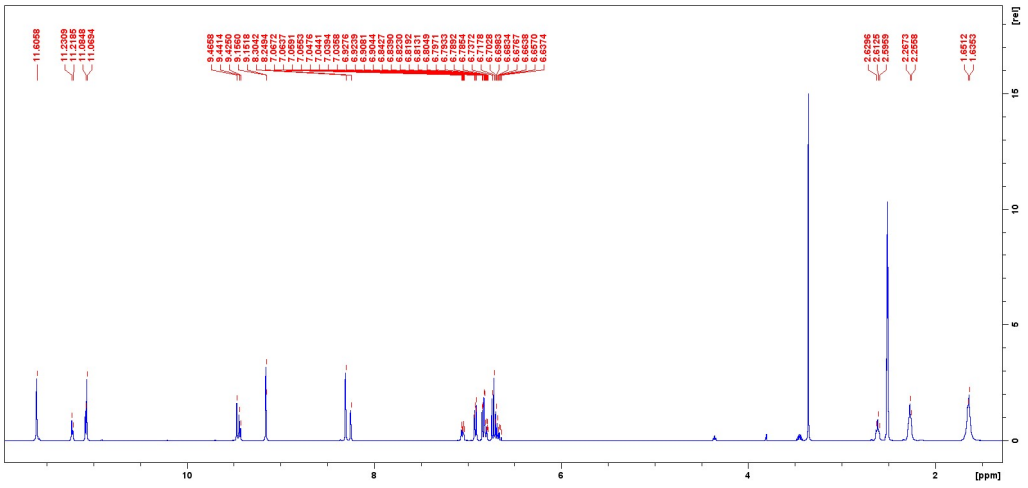

(c)

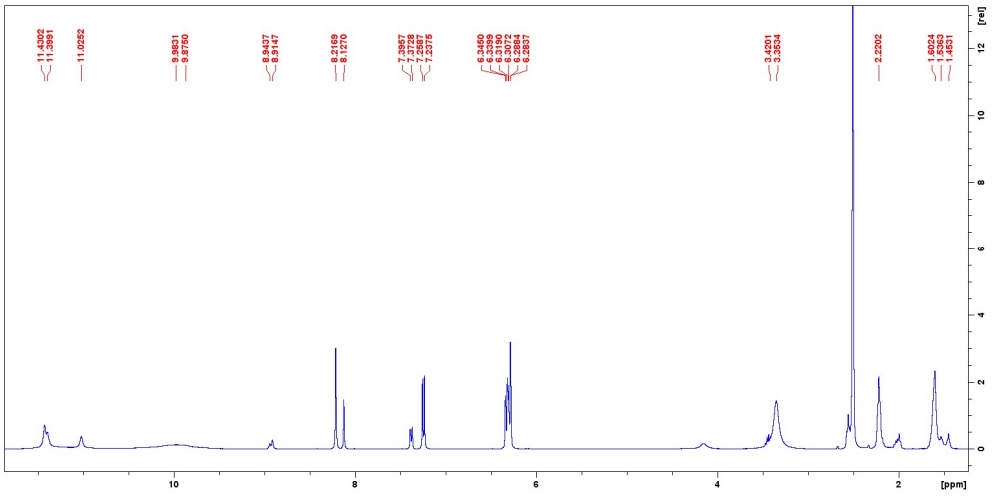

(d)

Figure S40. ^{1}H NMR spectra of a) $\mathbf{H_4L^5}$; b) $\mathbf{H_4L^6}$; c) $\mathbf{H_4L^7}$ and d) $\mathbf{H_4L^8}$ in DMSO-d_6, at 25 °C.

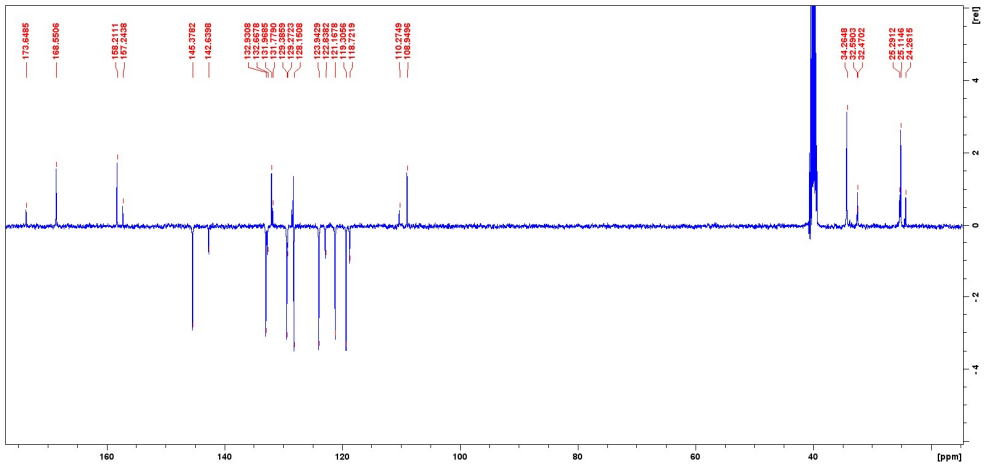
173.6485
168.5506
158.2111
157.2438
145.3782
142.6398
132.9308
132.6678
131.9685
131.7790
129.3859
129.2723
128.1508
123.9429
122.8382
121.1678
119.3056
118.7219
110.2749
108.9496
34.2648
32.5903
32.4702
25.2912
25.1146
24.2615
[rel]
[ppm]

(a)

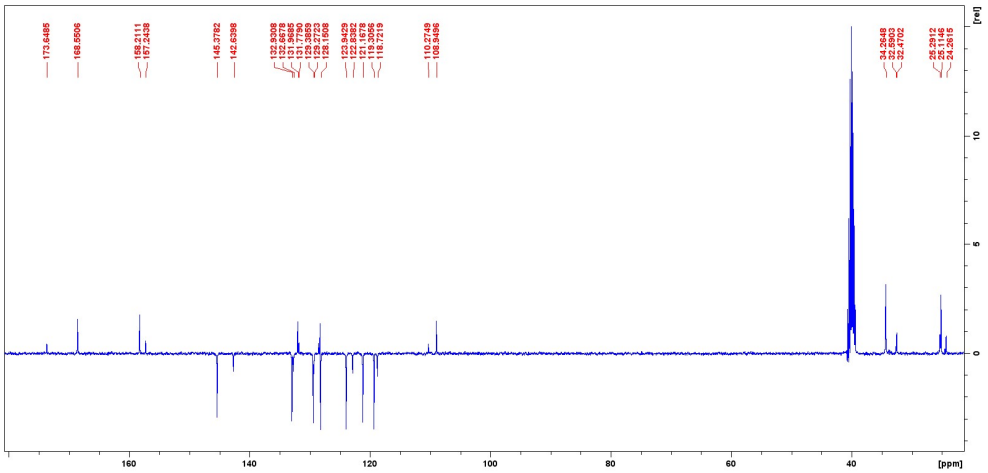
173.6485
168.5506
158.2111
157.2438
145.3782
142.6398
132.9308
132.6678
131.9685
131.7790
129.3859
129.2723
128.1508
123.9429
122.8382
121.1678
119.3056
118.7219
110.2749
108.9496
34.2648
32.5903
32.4702
25.2912
25.1146
24.2615
[rel]
[ppm]

(b)

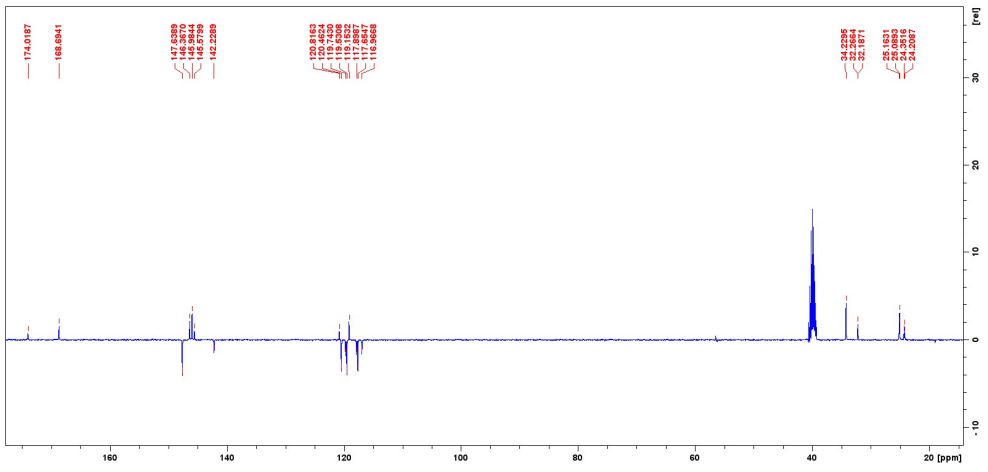
174.0187
168.6941
147.6389
146.3670
145.9944
145.5799
142.2289
120.8163
120.4624
119.7430
119.5308
119.1532
117.8987
117.6547
116.9668
34.2295
32.2664
32.1871
25.1631
25.0893
24.3516
24.2087
[rel]
[ppm]

(c)

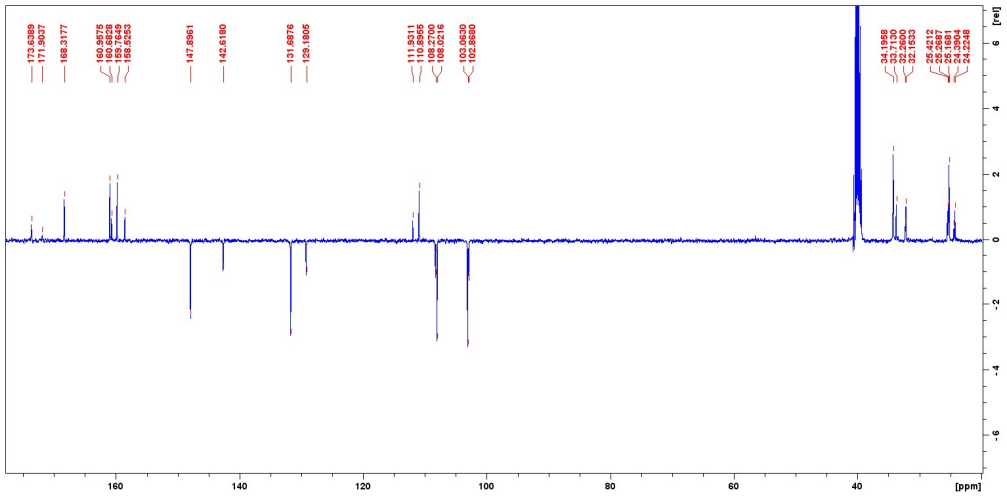

(d)

Figure S41. ^{13}C NMR spectra of a) $\mathbf{H_4L^5}$; b) $\mathbf{H_4L^6}$; c) $\mathbf{H_4L^7}$ and d) $\mathbf{H_4L^8}$ in DMSO-d_6, at 25 °C.

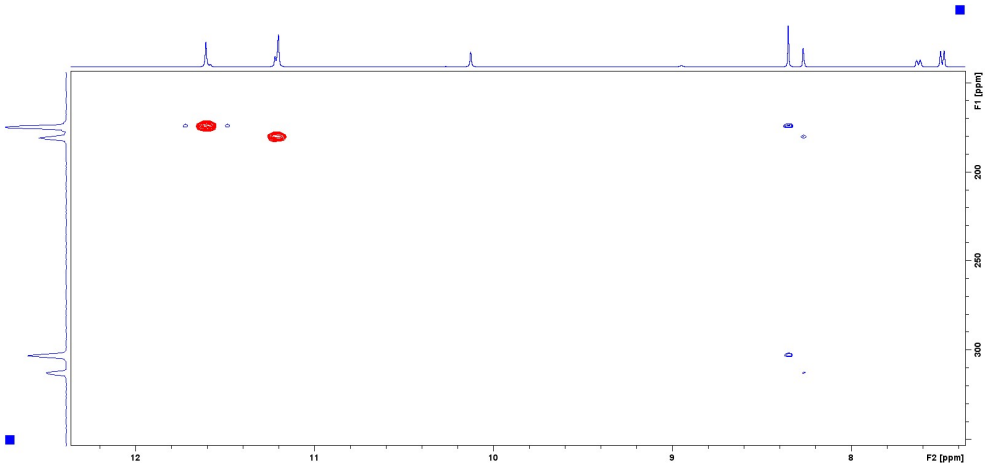
F1 [ppm]
200
250
300
12
11
10
9
8
F2 [ppm]

(a)

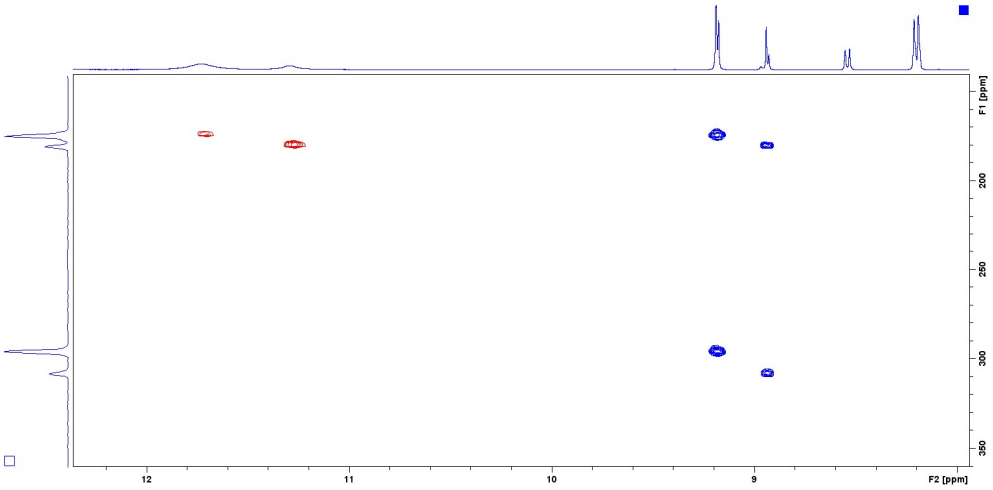
F1 [ppm]
200
250
300
350
12
11
10
9
F2 [ppm]

(b)

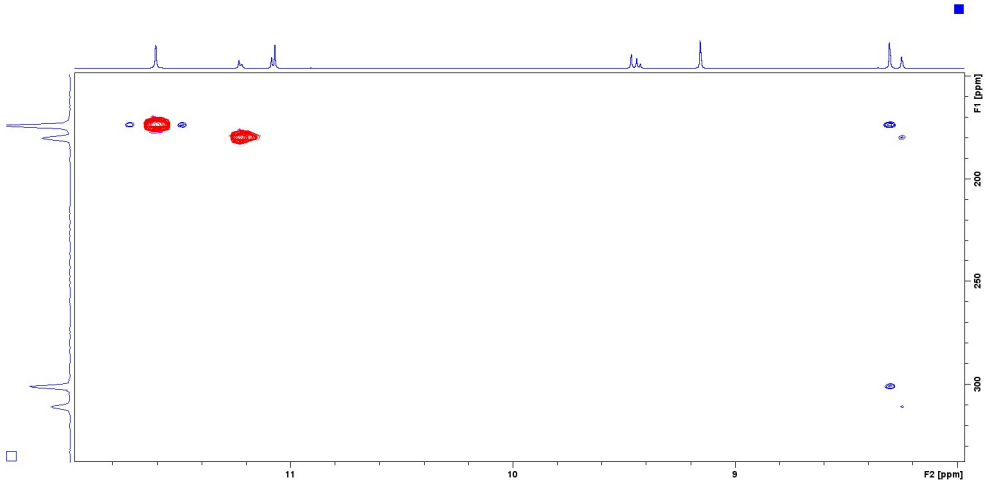
F1 [ppm]
200
250
300
11
10
9
F2 [ppm]

(c)

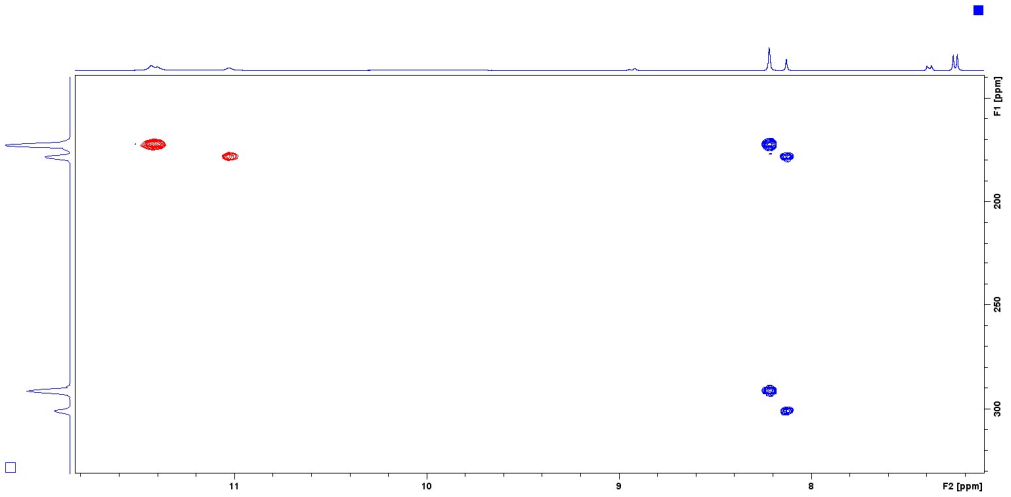

(d)

Figure S42. ^{1}H-^{15}N HSQC-HMBC overlay of spectra for a) $\mathbf{H_4L^5}$; b) $\mathbf{H_4L^6}$; c) $\mathbf{H_4L^7}$ and d) $\mathbf{H_4L^8}$ in DMSO-d_6, at 25 °C. In all cases ^{1}H-^{15}N HSQC signals are shown in red, whereas ^{1}H-^{15}N HMBC signals are shown in blue.

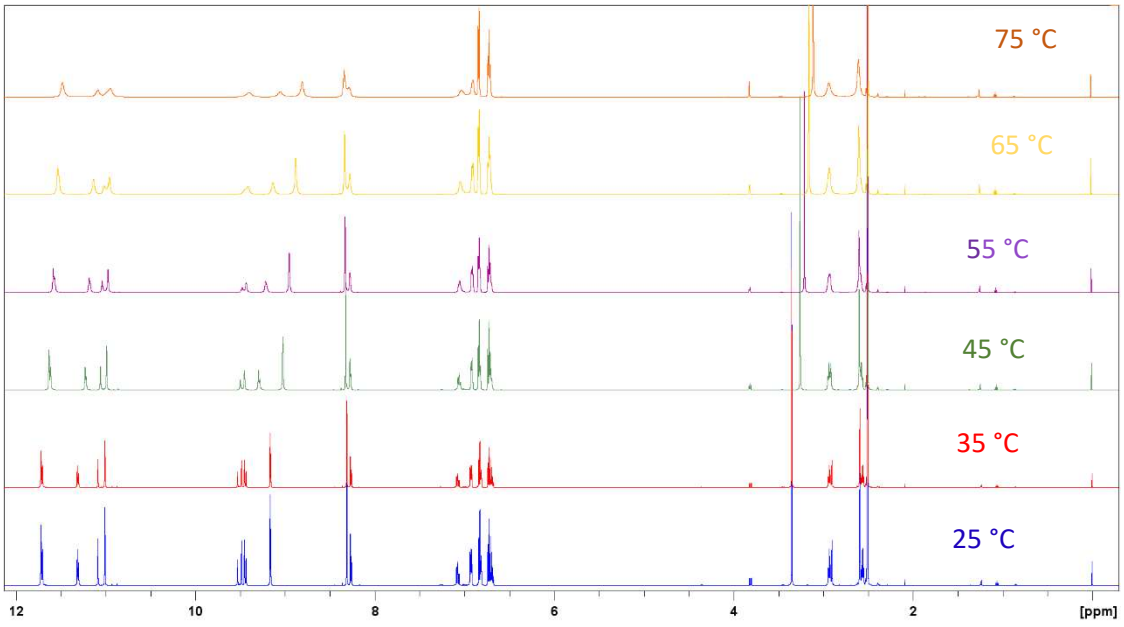
75 °C
65 °C
55 °C
45 °C
35 °C
25 °C
12
10
8
6
4
2
[ppm]

(a)

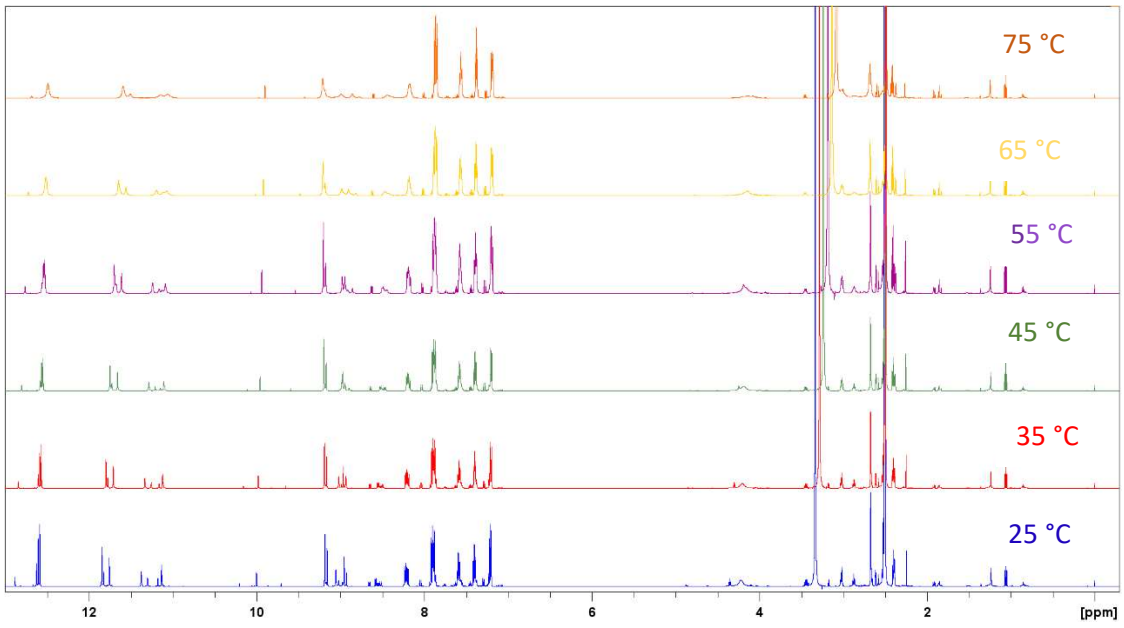
75 °C
65 °C
55 °C
45 °C
35 °C
25 °C
12
10
8
6
4
2
[ppm]

(b)

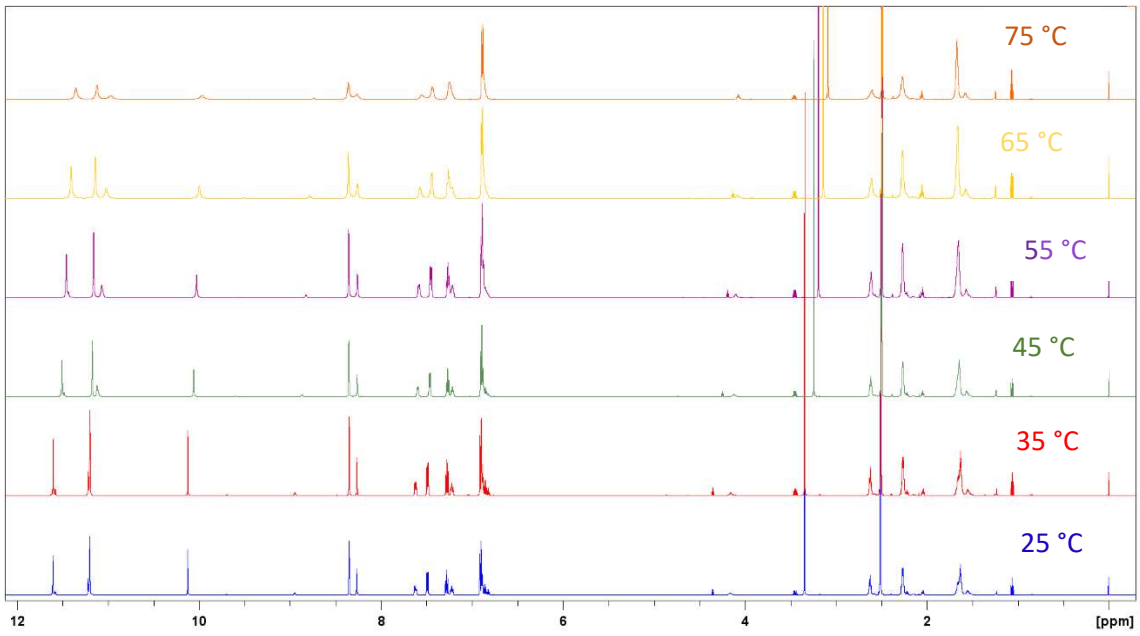

(c)

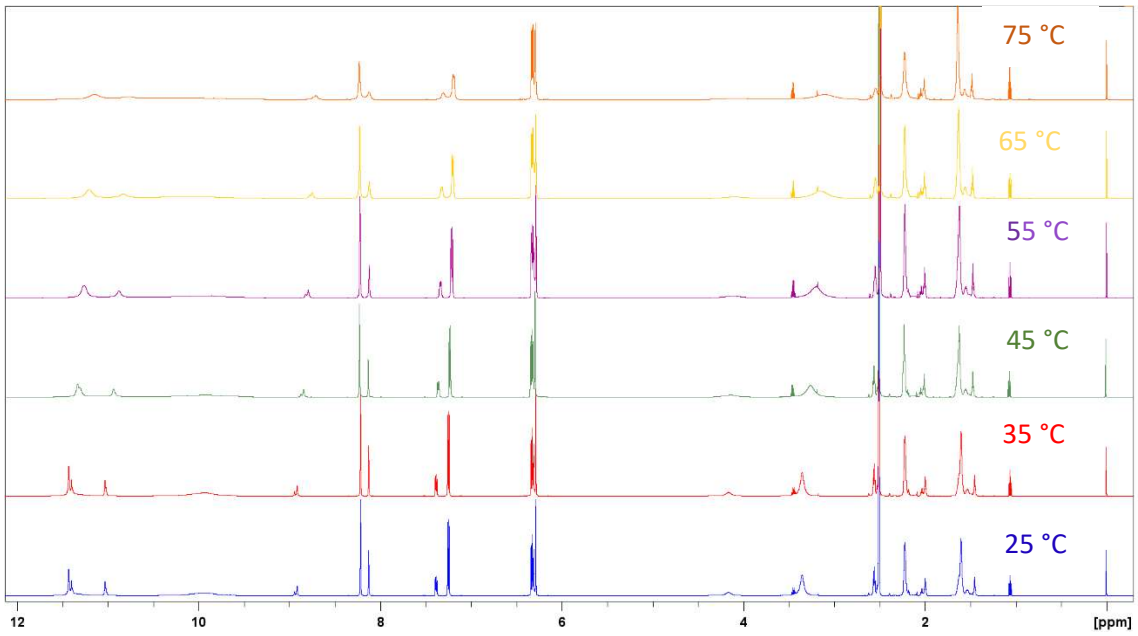

(d)

Figure S43. ^{1}H NMR spectra of: (a) $\mathbf{H_4L^1}$, (b) $\mathbf{H_4L^2}$, (c) $\mathbf{H_4L^3}$ and (d) $\mathbf{H_4L^4}$ in DMSO-d_6 solution at different temeperatures.

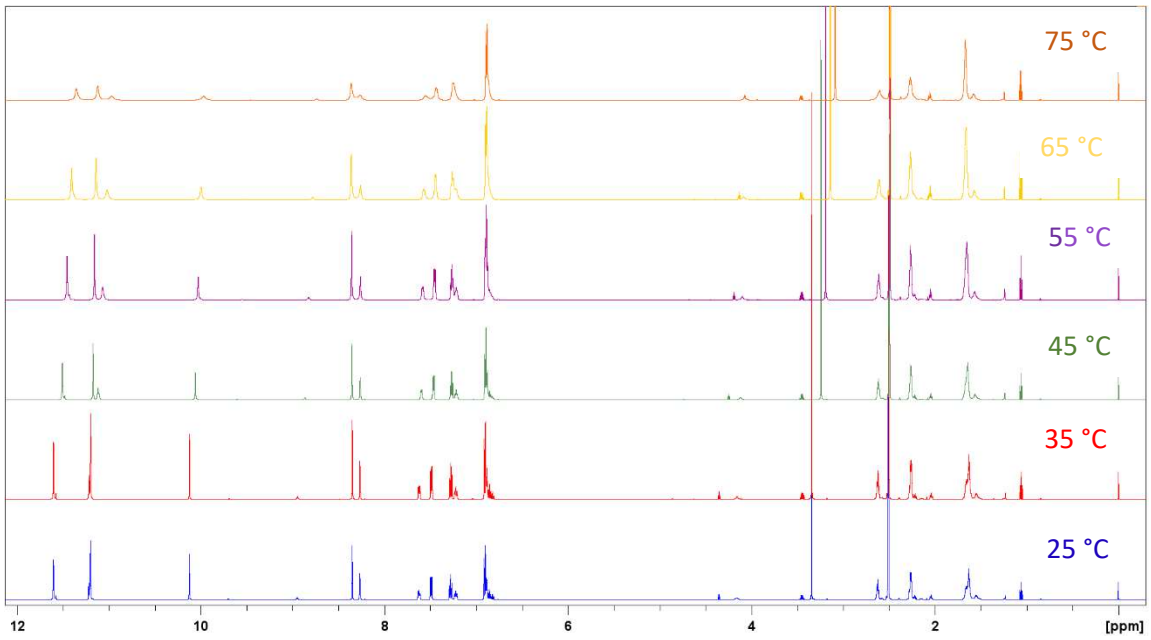
75 °C
65 °C
55 °C
45 °C
35 °C
25 °C
12
10
8
6
4
2
[ppm]

(a)

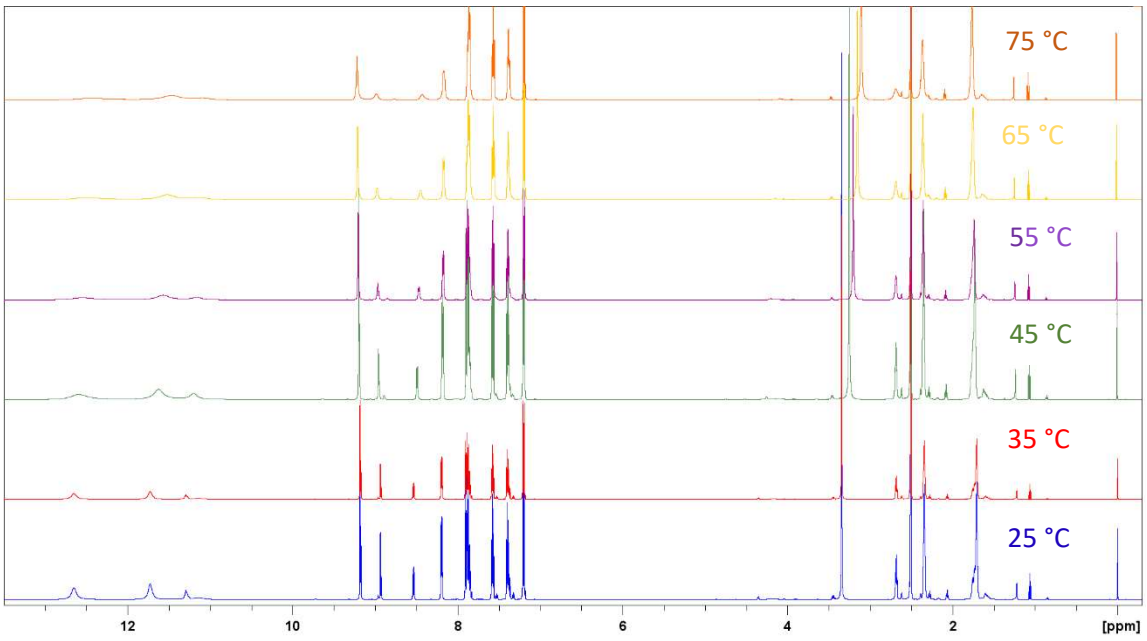
75 °C
65 °C
55 °C
45 °C
35 °C
25 °C
12
10
8
6
4
2
[ppm]

(b)

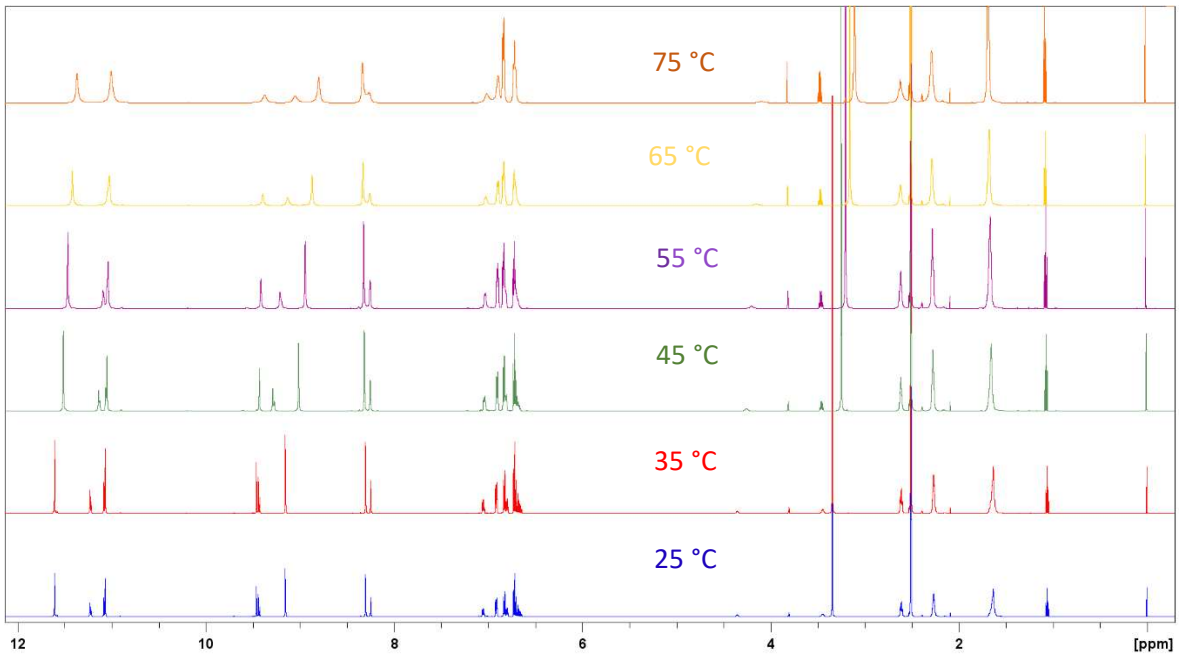

(c)

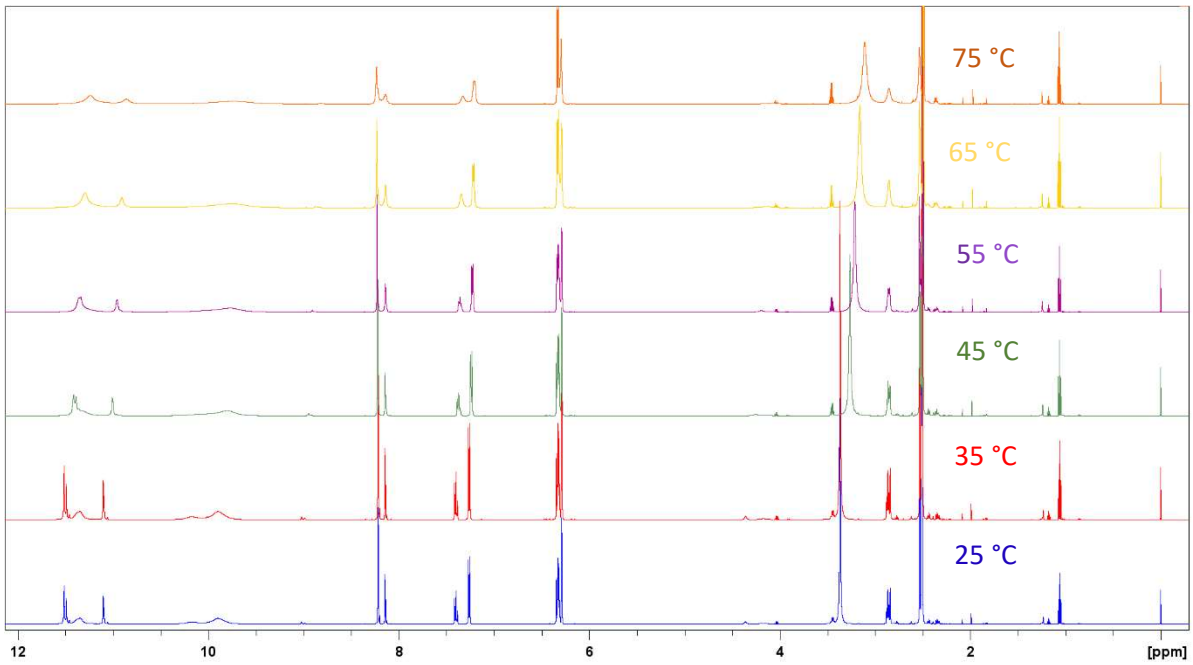

(d)

Figure S44. ^{1}H NMR spectra of: (a) $\mathbf{H_4L^5}$, (b) $\mathbf{H_4L^6}$, (c) $\mathbf{H_4L^7}$ and (d) $\mathbf{H_4L^8}$ in DMSO-d_6 solution at different temperatures.